Journal of Sound and Vibration 638 (2026) 119840

Contents lists available at ScienceDirect

Journal of Sound and Vibration

journal homepage: www.elsevier.com/locate/jsvi

On reflected waves in a semi-infinite string due to a boundary condition with a cubic nonlinearity

Jeri Araiku *, Wim T. van Horssen

Mathematical Physics, Delft Institute of Applied Mathematics, Faculty of EEMCS, Delft University of Technology, Mekelweg 5, Delft, 2628CD, South Holland, The Netherlands

ARTICLE INFO

2000 MSC:
35B20
35G30
37N99

Keywords:
Wave reflection
Nonlinear boundary condition
Multiple time-scales perturbation
D'Alembert method

ABSTRACT

In this paper, initial-boundary value problems (IBVPs) for a semi-infinite string with a tuned-mass-damper (TMD) system attached at one end are studied. While previous studies have focused primarily on the linear behavior of springs, we extend the analysis to include cubic nonlinearity. Four types of TMD system are considered, that is, a dashpot-linear spring, a mass-dashpot-linear spring, a dashpot-nonlinear spring, and a mass-dashpot-nonlinear spring, to assess wave reflections under these configurations. A key contribution of this research is that, rather than assuming predefined forms for the reflected wave, we derive the reflection shapes directly from calculations, offering new insights into wave dynamics. The D'Alembert formula is used to describe the general solution of the wave equation, accounting for the string's initial velocity and displacement. For the nonlinear cases, the Multiple Scales Perturbation (MSP) method is used to approximate solutions. Our results demonstrate that the mass, spring, and damper coefficients strongly influence the wave reflections. Additionally, adjusting the damping coefficient to small values reveals a completely different behavior of the reflected waves compared to large values. Numerical simulations using a fourth-order Runge-Kutta (RK4) method and a central finite difference scheme support the analytical results. Energy dissipation is studied for all scenarios, confirming that the solutions remain bounded over large timescales.

1. Introduction

All mechanical systems possessed of mass and stiffness are subject to vibrations [1]. Mechanical vibrations result from the oscillatory response of elastic bodies to internal or external forces. Undesired transverse vibrations of string systems are inevitable and can lead to discomfort and even destruction-for example, bridge collapses due to earthquakes or strong rain-wind phenomena. Hence, different tuned-mass-damper systems are installed to suppress the undesired oscillations of (for instance) a bridge. Due to their theoretical and practical importance, research on wave properties and their reflections has been one of the most exciting areas of research. Various applications in mechanical devices, such as cable-stayed bridges [2,3], elevator cables [4], musical instruments [5], marine cables [6,7], and power transmission lines [8,9], can be simplified and treated as strings for motion analysis purposes [10,11].

Simple models describing these vibrations can be formulated as initial-boundary-value problems (IBVPs) for a wave equation in the case of a string-like problem [12]. String problems with various initial conditions (ICs) have been analyzed [13–20]. Regarding boundaries, these studies focused primarily on scenarios in which one end is fixed while the other end consists of a spring, damper,

* Corresponding author.
E-mail addresses: J.Araiku@tudelft.nl (J. Araiku), W.T.vanHorssen@tudelft.nl (W.T. van Horssen).

https://doi.org/10.1016/j.jsv.2026.119840
Received 10 October 2025; Received in revised form 24 April 2026; Accepted 27 April 2026
Available online 28 April 2026

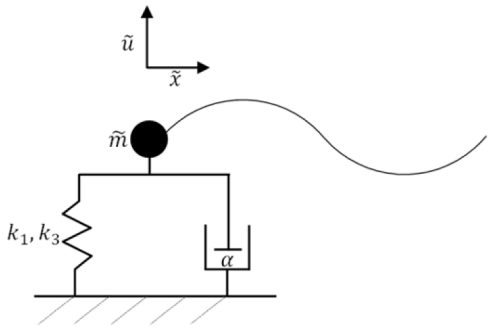

Fig. 1. The tuned mass damper (TMD) system at $\tilde{x} = 0$.

and lumped mass. In practical engineering systems, strings are finite in length, leading to wave reflections at both boundaries and complicating the analysis of boundary support effectiveness. However, this fixed-end configuration fails to accurately represent engineering practice due to the complexity of real-world working environments and the elasticity of support materials [21]. On the other hand, a semi-infinite string simplifies this by isolating the interaction with a single boundary. By analyzing the reflected wave profile and energy dissipation, this model provides insight into the efficiency of boundary support in suppressing vibration.

Akkaya and van Horssen [1,22] considered properties of reflection and damping for semi-infinite string equations using the D'Alembert method. However, the boundary conditions (BCs) for vibrating strings in these studies are primarily linear, excluding nonlinear effects. When nonlinear terms are introduced, obtaining exact analytical solutions for such systems is usually impossible, significantly increasing the complexity of the solution [23]. To address these complex boundary-value problems, researchers have turned to approximate analytical methods, with the Method of Multiple Scales being a notable example. This method provides a systematic framework for analyzing nonlinear vibration behavior and resonance-induced amplitude variations while ensuring uniformly valid approximations [24,25]. Darmawijoyo and van Horssen [12,20] also constructed asymptotic approximations to study such IBVPs for a weakly nonlinear string equation with a non-classical linear BC by a multiple scales perturbation (MSP) method.

Reflected waves in semi-infinite rods with a (non-)linear boundary stiffness have been investigated [26–29]. However, the authors assumed that the reflected wave takes a specific form. In this study, we will show that the waveforms are derived from our calculations and apply to all ICs. The main objective is to model and understand wave damping and reflection in semi-infinite strings by solving IBVPs for partial differential equations (PDEs). In this study, we will consider linear and nonlinear spring systems at the boundary. The well-known D'Alembert formula is used throughout this paper to describe the general solution of the wave equation with the corresponding initial velocity and displacement [30,31]. An MSP method is used to approximate the solution of the nonlinear problem.

This paper is organized as follows. In Section 2, we will introduce the IBVPs that describe the transverse vibrations of a semi-infinite string under different BCs. In this section, we also implement a simple rescaling to put the IBVP in a non-dimensional form. In Section 3, we will introduce the analysis method to address the problems identified in Section 2. In Section 4, we will study four types of TMD system: (1) no mass and a linear spring, (2) no mass and a nonlinear spring, (3) a mass with a linear spring, and (4) a mass with a nonlinear spring. For the last type of BC, we also consider two cases for the damping coefficient: a large one and a small one. For the nonlinear parts, we are using the MSP method to approximate the solutions. In Section 5, the total energy and its rate of change in time are presented for the different cases studied in Section 3. Finally, in Section 6, conclusions are drawn, and suggestions for future research are discussed.

2. Formulation of the model

In this paper, we consider a TMD system attached to one end of a semi-infinite string-like material as shown in Fig. 1, where $\tilde{u}$ and $\tilde{x}$ are the vertical displacement and the horizontal coordinate, respectively, $c^2 = \frac{\mathcal{T}}{\rho}$ is the wave velocity, $\mathcal{T}$ is the (assumed) constant tension in the string, ρ is the mass-density of the string, $\tilde{t}$ is time, $\tilde{m}$ is a mass, k_1 and k_3 are the linear and cubic nonlinear stiffness coefficients of the spring, α is a damping coefficient, $\tilde{f}$ is the initial vertical displacement of the string, and $\tilde{g}$ is the initial vertical velocity of the string. All constants are non-negative. We will consider a string of semi-infinite length, extending in the positive direction from $\tilde{x} = 0$, where at $\tilde{x} = 0$ a TMD system has been attached.

The IBVP is given by:

$$\begin{aligned}
&\text{PDE:} \quad \tilde{u}_{\tilde{t}\tilde{t}} - c^2\tilde{u}_{\tilde{x}\tilde{x}} = 0, \quad \tilde{x} > 0, \quad \tilde{t} > 0,\\
&\text{ICs:} \quad \tilde{u}(\tilde{x},0) = \tilde{f}(\tilde{x}), \quad \tilde{u}_{\tilde{t}}(\tilde{x},0) = \tilde{g}(\tilde{x}), \ \tilde{x} \geq 0,\\
&\text{BC:} \quad \tilde{m}\tilde{u}_{\tilde{t}\tilde{t}}(0,\tilde{t}) = \mathcal{T}\tilde{u}_{\tilde{x}}(0,\tilde{t}) - k_1\tilde{u}(0,\tilde{t}) - k_3\tilde{u}^3(0,\tilde{t}) - \alpha\tilde{u}_{\tilde{t}}(0,\tilde{t}), \ \tilde{t} \geq 0.
\end{aligned} \tag{1}$$

To put the IBVP (1) in a non-dimensional form, we use the following dimensionless quantities:

$$\tilde{x} = xL, \quad \tilde{t} = tT, \quad \tilde{u} = uL, \quad \tilde{f} = fL, \quad \tilde{g} = \frac{gL}{T},$$

where L and T are some dimensional characteristic quantities for length and time, respectively. By inserting these non-dimensional quantities into (1), we obtain the following dimensionless IBVP:

$$\begin{aligned}
&\text{PDE:}\quad u_{tt}-u_{xx}=0,\quad x>0,\quad t>0,\\
&\text{ICs:}\quad u(x,0)=f(x),\quad u_t(x,0)=g(x),\quad x\geq 0,\\
&\text{BC:}\quad \begin{cases} u_{tt}(0,t)=u_x(0,t)-pu(0,t)-\varepsilon u^3(0,t)-\beta u_t(0,t), & (\text{for}\quad \tilde{m}>0),\\ u_x(0,t)=\tilde{\beta}u_t(0,t)+\tilde{p}u(0,t)+\tilde{\varepsilon}u^3(0,t), & (\text{for}\quad \tilde{m}=0),\end{cases}\\
&\text{for}\quad t\geq 0,\quad \beta\geq 0,\quad p\geq 0,\quad \varepsilon\geq 0,\quad \tilde{\beta}\geq 0,\quad \tilde{p}\geq 0,\quad \tilde{\varepsilon}\geq 0,
\end{aligned}\tag{2}$$

where $f\in C^2$ and $g\in C^1$, with $\frac{c^2T^2}{L^2}=1$. For $\tilde{m}>0$, we choose $\frac{\mathcal{T}T^2}{\tilde{m}L}=1$, $k_3=\frac{\tilde{m}}{LT^2}$, $p=\frac{k_1c}{\mathcal{T}}$, $\varepsilon=\frac{k_3L^2T^2}{\tilde{m}}$, and $\beta=\frac{\alpha c}{\mathcal{T}}$. For $\tilde{m}=0$, we choose $\tilde{\beta}=\frac{\alpha L}{\mathcal{T}}$, $\tilde{p}=\frac{k_1L}{\mathcal{T}}$, and $\tilde{\varepsilon}=\frac{k_3L^3}{\mathcal{T}}$. We assume that $0\leq\varepsilon\ll 1$ and $0\leq\tilde{\varepsilon}\ll 1$. For convenience, we drop the 'tilde' sign for the $\tilde{m}=0$ problems in (2).

A similar study was conducted by Akkaya and van Horssen in [32], focusing on linear problems. In that study, f and g are considered to be two independent functions. However, from a physical perspective, this is not always applicable. For example, when we consider our ICs in (2), when $x=0$:

$$\begin{aligned}
u(x,0)=f(x)&\to u(0,0)=f(0),\\
u_x(x,0)=f_x(x)&\to u_x(0,0)=f_x(0),\\
u_{xx}(x,0)=f_{xx}(x)&\to u_{xx}(0,0)=f_{xx}(0),\\
u_t(x,0)=g(x)&\to u_t(0)=g(0),
\end{aligned}\tag{3}$$

and from the first BC in (2), it then follows for $t=0$ that

$$f_{xx}(0)=f_x(0)-pf(0)-\varepsilon(f(0))^3-\beta g(0),\quad \beta\geq 0,\quad p\geq 0,\quad \varepsilon\geq 0.\tag{4}$$

From Eq. (4), we can see that f and g depend on each other. Therefore, in this study, f and g are not treated as two independent functions. Consequently, the solutions provided in this paper are applicable to a larger class of ICs (including linear BCs).

3. Method of analysis

In this study, we will examine four distinct problems, specifically addressing the following scenarios:

1. $\tilde{m}=0,\varepsilon=0$,
2. $\tilde{m}\neq 0,\varepsilon=0$,
3. $\tilde{m}=0,\varepsilon\neq 0$,
4. $\tilde{m}\neq 0,\varepsilon\neq 0$.

The well-known D'Alembert formula [30] is used to construct the solution.

$$u(x,t)=\begin{cases} \frac{1}{2}f(x+t)+\frac{1}{2}f(x-t)+\frac{1}{2}\int_{x-t}^{x+t}g(s)\,\mathrm{d}s, & \text{for } x-t>0,\\ \frac{1}{2}f(x+t)+\frac{1}{2}\int_0^{x+t}g(s)\,\mathrm{d}s+\frac{1}{2}f(x-t)-\frac{1}{2}\int_0^{x-t}g(s)\,\mathrm{d}s, & \text{for } x-t<0.\end{cases}\tag{5}$$

The D'Alembert method was chosen for its straightforwardness and sophistication. Specifically, this method, grounded in wave propagation, facilitates a more straightforward physical interpretation. Additionally, it does not require information on the frequency spectrum and eigenfunctions. Furthermore, this approach is well-suited not only to classical BCs but also to non-classical ones [33]. Note that the formula for $(x-t)<0$ is not defined for the negative arguments, since the ICs are only defined for the positive arguments, as we can see from (2). Although the physical domain is restricted to $x\geq 0$, the reflected wave is represented by extending the solution to $x<0$ using the method of images. This extension does not correspond to a physical medium in the negative spatial domain but serves as a mathematical construction that enforces the BC at $x=0$. By defining a suitable symmetric or antisymmetric continuation of the incident wave across the boundary, the superposition of incident and image waves yields the correct reflected wave when the solution is restricted back to the physical domain. This approach is standard in D'Alembert-type formulations and provides an exact representation of wave reflection at boundaries.

Let us define

$$\psi(x+t)=\frac{1}{2}f(x+t)+\frac{1}{2}\int_0^{x+t}g(s)\,\mathrm{d}s,\tag{6}$$

for $x-t<0$ and $x-t<s<0$,

$$\phi(t-x)=\frac{1}{2}f(x-t)-\frac{1}{2}\int_0^{x-t}g(s)\,\mathrm{d}s.\tag{7}$$

In this study, $\phi(t-x)$ denotes the unknown function we seek. We will formulate the problem for $\phi(t-x)$ as a problem for an Ordinary Differential Equation (ODE), and we will express the solution in the known function $\psi(x+t)$. Hence, our general solution

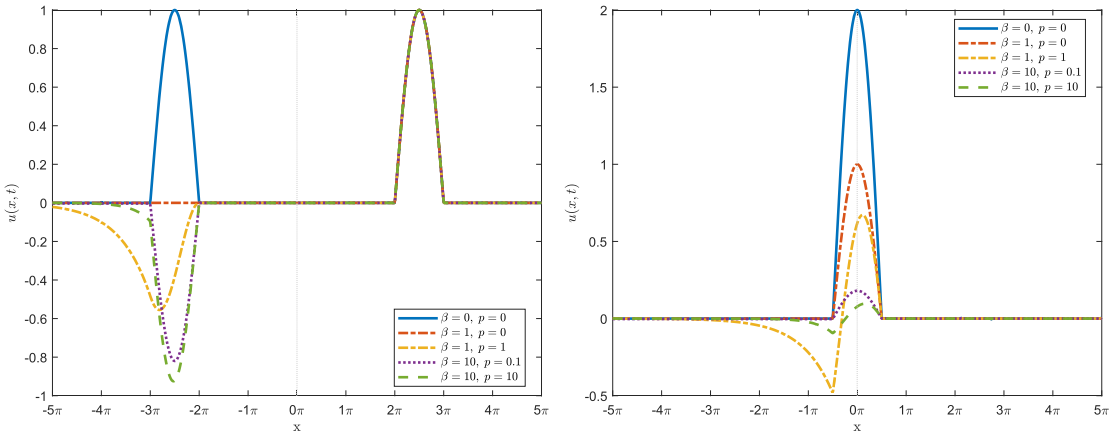

Fig. 2. A single sine wave and its reflections for the problem with $\tilde{m} = 0$, $\varepsilon = 0$, for different values of β and p at time: (a) $t = 0$ and (b) $t = \frac{5}{2}\pi$.

is given by

$$u(x,t) = \begin{cases} \frac{1}{2}f(x+t) + \frac{1}{2}f(x-t) + \frac{1}{2}\int_{x-t}^{x+t} g(s)\,\mathrm{d}s, & x-t>0, \\ \frac{1}{2}f(x+t) + \frac{1}{2}\int_{0}^{x+t} g(s)\,\mathrm{d}s + \phi(t-x), & x-t<0. \end{cases} \tag{8}$$

Nevertheless, it is usually unfeasible to obtain the exact solution for a nonlinear problem. Therefore, an accurate approximation is required for this problem. To approximate the solution of the nonlinear problem ($\varepsilon \neq 0$), we will use the MSP method.

4. Analysis

4.1. The problem with $\tilde{m} = 0$ and $\varepsilon = 0$

This problem is similar to [32], where it is assumed that f and g are independent of each other at $x = 0$. However, we will extend the problem to the case where f and g are not independent at $x = 0$.

The exact solution for $u(x,t)$ can be determined by substituting the D'Alembert formula (5) into BC (2) for $\tilde{m} = 0$ and $\varepsilon = 0$. Hence, we obtain the following first-order ODE yielding

$$(1+\beta)\phi'(t) + p\phi(t) = \frac{1-\beta}{2}\big(f'(t) + g(t)\big) - \frac{p}{2}\left(f(t) + \int_0^t g(s)\mathrm{d}s\right), \tag{9}$$

where the unknown function $\phi(t)$ for $x - t < 0$ is defined in (7). This ODE is readily solved using the integrating factor method. Replacing t by $t - x$, the expression for $\phi(t-x)$ in our solution (8) is given by

$$\begin{aligned} \phi(t-x) = {} & \frac{\beta}{1+\beta} f(0)\mathrm{e}^{\frac{p(x-t)}{1+\beta}} + \frac{1-\beta}{2(1+\beta)} f(t-x) - \frac{1}{2}\int_0^{t-x} g(s)\,\mathrm{d}s \\ & - \frac{p}{(1+\beta)^2}\mathrm{e}^{\frac{p(x-t)}{1+\beta}} \int_0^{t-x} f(s)\mathrm{e}^{\frac{ps}{1+\beta}}\,\mathrm{d}s + \frac{1}{1+\beta}\mathrm{e}^{\frac{p(x-t)}{1+\beta}} \int_0^{t-x} g(s)\mathrm{e}^{\frac{ps}{1+\beta}}\,\mathrm{d}s. \end{aligned} \tag{10}$$

This result confirms the results obtained in [22].

To observe how a wave reflects at the boundary $x = 0$, we select a single sine wave as IC, that is,

$$f(x) = \begin{cases} 0, & 0 < x < 2\pi, \\ \sin(x), & 2\pi \le x \le 3\pi, \\ 0, & 3\pi < x. \end{cases}; \quad g(x) = \begin{cases} 0, & 0 < x < 2\pi, \\ \cos(x), & 2\pi \le x \le 3\pi, \\ 0, & 3\pi < x. \end{cases} \tag{11}$$

Fig. 2a shows how the incoming wave ($x > 0$) and the reflected wave ($x < 0$) behave according to the solution (10) and the ICs (11). At the free end ($\beta \to 0$ and $p \to 0$), the reflection exhibits an even extension. The interaction between incident and reflected waves at $t = \frac{5\pi}{2}$ (Fig. 2b) results in a doubling of the wave amplitude (blue line). As the spring and damping coefficients increase, the reflected waves become more stretched and distorted. The fixed boundary ($\beta \to \infty$ or $p \to \infty$) produces an odd extension in the reflection. Consequently, at $t = \frac{5\pi}{2}$, the reflected wave interacts with the incoming wave at the boundary, momentarily resulting in a near 'flat line' appearance (purple and green lines). We identify the ideal damping condition for $\beta = 1$ and $p = 0$. Under this condition, the incoming wave is completely absorbed, preventing any deformation of the reflected wave (red line). Furthermore, we observe that the interaction between the spring and the damper distorts and elongates the reflected waves.

4.2. The problem with $\tilde{m} \neq 0$ and $\varepsilon = 0$

This problem is similar to [32]. Again, we extend the solution to include g. By substituting (5) into BC (2), it follows that $\phi(t)$ has to satisfy

$$\phi''(t) + (1+\beta)\phi'(t) + p\phi(t) = \gamma(t), \tag{12}$$

where

$$\gamma(t) = -\frac{f''(t)}{2} - \frac{g'(t)}{2} + \frac{(1-\beta)\big(f'(t)+g(t)\big)}{2} - \frac{p\Big(f(t)+\int_0^t g(s)\,\mathrm{d}s\Big)}{2}. \tag{13}$$

Eq. (12) yields two roots, $\lambda_{1,2} = \frac{-(1+\beta)\pm\sqrt{(1+\beta)^2-4p}}{2}$. The behavior of the system depends entirely on the values of p and β. Specifically, whether the system experiences over-damping ($(1+\beta)^2 > 4p$), critical damping ($(1+\beta)^2 = 4p$), or under-damping ($(1+\beta)^2 < 4p$) [34].

4.2.1. The case $(1+\beta)^2 > 4p$

There are two distinct real roots. Applying the method of variation of parameters to (12) yields:

$$\phi(t) = k_1 \mathrm{e}^{\lambda_1 t} + k_2 \mathrm{e}^{\lambda_2 t} - \frac{\mathrm{e}^{\lambda_1 t}\int_0^t \mathrm{e}^{-\lambda_1 s}\gamma(s)\,\mathrm{d}s}{(\lambda_2-\lambda_1)} + \frac{\mathrm{e}^{\lambda_2 t}\int_0^t \mathrm{e}^{-\lambda_2 s}\gamma(s)\,\mathrm{d}s}{(\lambda_2-\lambda_1)}. \tag{14}$$

Taking $t = 0$, and it follows from (7), we find

$$k_1 = \frac{(1-\lambda_1+\lambda_2)f(0)+g(0)}{2(\lambda_2-\lambda_1)} \quad \text{and} \quad k_2 = \frac{(-1-\lambda_1+\lambda_2)f(0)-g(0)}{2(\lambda_2-\lambda_1)}.$$

Given (13) for $\gamma(t)$ and applying integration by parts, we find $\phi(x-t)$ in (8),

$$\phi(t-x) = -\frac{1}{2}f(t-x) + \frac{f(0)}{2}\sum_{i=1}^{2}\Lambda_i \mathrm{e}^{\lambda_i(t-x)} - \sum_{i=1}^{2}\frac{(-1)^i \mathrm{e}^{\lambda_i(t-x)}}{2(\lambda_2-\lambda_1)}\left[\int_0^{t-x}\mathrm{e}^{-\lambda_i s}\left(a_i f(s) + b_i g(s) + p\int_0^s g(v)\,\mathrm{d}v\right)\mathrm{d}s\right], \tag{15}$$

where for $i = 1, 2$, $\Lambda_i = 1 + (-1)^i \cdot \frac{\beta-1}{\lambda_2-\lambda_1}$; $a_i = \lambda_i^2 + (\beta-1)\lambda_i + p$; $b_i = \lambda_i + \beta - 1$.

4.2.2. The case $(1+\beta)^2 = 4p$

There is a double real root λ. Again, applying the method of variation of parameters yields the following

$$\phi(t) = k_3\mathrm{e}^{-\theta t} + k_4 t\mathrm{e}^{-\theta t} - \mathrm{e}^{-\theta t}\int_0^t s\mathrm{e}^{\theta s}\gamma(s)\,\mathrm{d}s + t\mathrm{e}^{-\theta t}\int_0^t \mathrm{e}^{\theta s}\gamma(s)\,\mathrm{d}s, \tag{16}$$

with $\theta = \frac{1+\beta}{2}$.

For $t = 0$, we find $k_3 = \frac{1}{2}f(0)$ and $k_4 = \frac{1}{2}\theta f(0) + \frac{1}{2}g(0)$. Taking into account (13) for $\gamma(t)$ and applying integration by parts, we obtain the solution $\phi(\hat{t})$ with $\hat{t} = t - x$,

$$\begin{aligned}\phi(\hat{t}) = -\tfrac{f(\hat{t})}{2} + \mathrm{e}^{-\theta(\hat{t})}\Bigg\{&\big[1+(\theta-1)(\hat{t})\big]f(0) + g(0)\hat{t} + \Big(1 + \tfrac{\theta(\beta-3)-2p}{4}(\hat{t})\Big)\int_0^{\hat{t}}\mathrm{e}^{\theta s}f(s)\,\mathrm{d}s + \Big(\tfrac{\theta(3-\beta)+2p}{4}\Big)\int_0^{\hat{t}} s\mathrm{e}^{\theta s}f(s)\,\mathrm{d}s \\ &- \Big(\tfrac{1}{2} + \tfrac{\beta-3}{4}(\hat{t})\Big)\int_0^{\hat{t}}\mathrm{e}^{\theta s}g(s)\,\mathrm{d}s + \tfrac{\beta-3}{4}\int_0^{\hat{t}} s\mathrm{e}^{\theta s}g(s)\,\mathrm{d}s + \tfrac{1}{2}p\left[\int_0^{\hat{t}} s\mathrm{e}^{\theta s}\Big(\int_0^s g(v)\,dv\Big)\mathrm{d}s - (\hat{t})\int_0^{\hat{t}}\mathrm{e}^{\theta s}\Big(\int_0^s g(v)\,dv\Big)\mathrm{d}s\right]\Bigg\}.\end{aligned} \tag{17}$$

4.2.3. The case $(1+\beta)^2 < 4p$

In this case, λ is complex valued. The general solution for $\phi(t)$ (13) is obtained by using the method of variation of parameters, resulting in

$$\phi(t) = \mathrm{e}^{-\theta t}\big\{k_5\cos(\kappa t) + k_6\sin(\kappa t) - \frac{\cos(\kappa t)}{\kappa}\int_0^t \mathrm{e}^{\theta s}\sin(\kappa s)\gamma(s)\mathrm{d}s + \frac{1}{\kappa}\sin(\kappa t)\int_0^t \mathrm{e}^{\theta s}\cos(\kappa s)\gamma(s)\mathrm{d}s\big\}, \tag{18}$$

with $\kappa = \frac{\sqrt{4p-(1+\beta)^2}}{2}$ and $\theta = \frac{(1+\beta)}{2}$. Taking $t = 0$, we have $\phi(0) = \frac{1}{2}f(0)$ and $\phi'(0) = -\frac{1}{2}f'(0) + \frac{1}{2}g(0)$, then we find $k_5 = \frac{1}{2}f(0)$ and $k_6 = \frac{\theta f(0)-g(0)}{2\kappa}$. Applying integration by parts, we can find the expression for $\phi(\hat{t})$ in (8),

$$\begin{aligned}\phi(\hat{t}) = -\frac{1}{2}f(\hat{t}) + \mathrm{e}^{\hat{t}}\Bigg[&\Big(\cos(\kappa\hat{t}) + \frac{\beta-1}{2\kappa}\sin(\kappa\hat{t})\Big)f(0) + \frac{1}{2\kappa}\sin(\kappa\hat{t})\,g(0) \\ &+ \Big(\cos(\kappa\hat{t}) - \frac{\theta}{\kappa}\sin(\kappa\hat{t})\Big)F_c(\hat{t}) + \Big(\sin(\kappa\hat{t}) + \frac{\theta}{\kappa}\cos(\kappa\hat{t})\Big)F_s(\hat{t}) \\ &- \Big(\frac{\cos(\kappa\hat{t})}{2} - \frac{3-\beta}{4\kappa}\sin(\kappa\hat{t})\Big)G_c(\hat{t}) - \Big(\frac{\sin(\kappa\hat{t})}{2} + \frac{3-\beta}{4\kappa}\cos(\kappa\hat{t})\Big)G_s(\hat{t}) + \frac{p}{2\kappa}\Big(\cos(\kappa\hat{t})\,H_s(\hat{t}) - \sin(\kappa\hat{t})\,H_c(\hat{t})\Big)\Bigg],\end{aligned} \tag{19}$$

with $\hat{t} = t - x$. The definitions of $F_c(\hat{t}), F_s(\hat{t}), G_c(\hat{t}), G_s(\hat{t}), H_c(\hat{t})$, and $H_s(\hat{t})$ can be found in Appendix A.

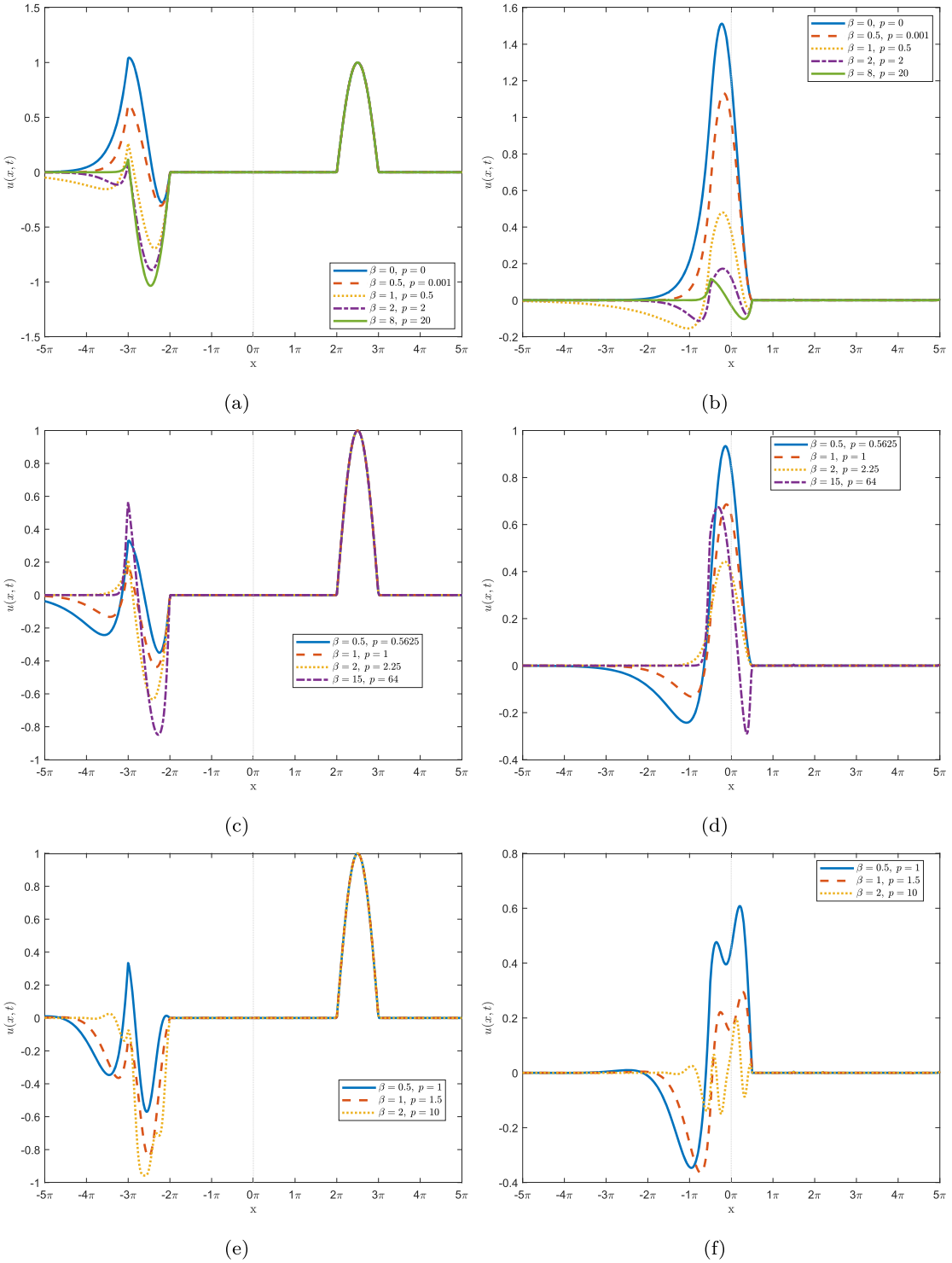

Fig. 3. A single sine wave and its reflections for $\tilde{m} \neq 0$ and $\varepsilon = 0$ with different values of the parameters β and p. For the case $(1+\beta)^2 > 4p$ at time: (a) $t = 0$ and (b) $t = \frac{5\pi}{2}$. For the case $(1+\beta)^2 = 4p$ at time: (c) $t = 0$ and (d) $t = \frac{5\pi}{2}$. For the case $(1+\beta)^2 < 4p$ at time: (e) $t = 0$ and (f) $t = \frac{5\pi}{2}$.

We take f and g in (11) as ICs to visualize the solution and how the reflected waves behave (see Fig. 3). In all cases, we can see that the behavior of the solutions differs as the damping parameter β and the linear spring coefficient p vary. As in the first problem (Section 4.1), when the string can move freely in the $u-$direction at the boundary, the extension of the reflected waves becomes even, and odd when the string is fixed at the boundary. These findings validate the conclusions presented in [32]. Furthermore, it is observed that the wavelength not only extends but also undergoes significant deformation relative to the incident wave. This transformation arises due to complex interactions among the mass, spring, and dashpot during the reflection process [33].

We also illustrate how the wave transitioned at the boundary at $t = \frac{5\pi}{2}$ (Fig. 3b, d, and f). This finding is consistent with the observations of [35], which indicate that vibration amplitudes may increase or decrease over time depending on the stiffness coefficient of the coupled mass-spring-damper system.

4.3. The problem with $\tilde{m} = 0$ and $\varepsilon \neq 0$

In this section, we study how reflected waves behave when the boundary acts nonlinearly. First, we consider the damping-spring system without mass ($\tilde{m} = 0$). Hence, we have the following BC for the system (2):

$$u_x(0,t) = \beta u_t(0,t) + pu(0,t) + \varepsilon u^3(0,t). \tag{20}$$

Using our definitions (6) and (7) for $\psi(t)$ and $\phi(t)$ in D'Alembert's general solution (5), and substituting this solution into the BC (20), we obtain

$$(1-\beta)\psi'(t) - p\psi(t) - \varepsilon\psi^3(t) = (1+\beta)\phi'(t) + p\phi(t) + \varepsilon(\phi^3(t) + 3\phi^2(t)\psi(t) + 3\phi(t)\psi^2(t)), \tag{21}$$

where $\psi(t)$ is a known function and $\phi(t)$ is an unknown function.

It is usually impossible to find the exact solution of the nonlinear Eq. (21) for $\phi(t)$. Therefore, we will be looking for an accurate approximation of the unknown function $\phi(t-x)$ in (8), denoted by $\phi_a(t-x)$. Then, the approximation of the solution for the displacement $u(x,t)$ is given by

$$u(x,t) = \begin{cases} \frac{1}{2}f(x+t) + \frac{1}{2}f(x-t) + \frac{1}{2}\int_{x-t}^{x+t} g(s)\,\mathrm{d}s, & \text{for } x-t>0, \\ \frac{1}{2}f(x+t) + \frac{1}{2}\int_{0}^{x+t} g(s)\,\mathrm{d}s + \phi_a(t-x), & \text{for } x-t<0. \end{cases} \tag{22}$$

We will do this by using the MSP method. We start by introducing a slow time scale τ, defined as $\tau = \varepsilon t$. This allows us to express an asymptotic expansion for $\phi(t)$ as follows:

$$\phi(t) = \hat{\phi}(t,\tau) = \hat{\phi}_0(t,\tau) + \varepsilon\hat{\phi}_1(t,\tau) + \varepsilon^2\hat{\phi}_2(t,\tau) + \cdots \tag{23}$$

For our convenience, we will drop the 'hat' sign. Substituting (23) into (21), we derive the following equations of $\mathcal{O}(1)$, and of $\mathcal{O}(\varepsilon)$:

$$\begin{cases} \mathcal{O}(1): & (1+\beta)\phi_{0_t} + p\phi_0 = (1-\beta)\psi'(t) - p\psi(t) = \psi_0(t), \\ \mathcal{O}(\varepsilon): & (1+\beta)\phi_{1_t} + p\phi_1 = -(1+\beta)\phi_{0_{t\tau}} - (\hat{\phi}_0 + \psi(t))^3. \end{cases} \tag{24}$$

From the first equation in (24), it follows that:

$$\phi_0(t,\tau) = \mathcal{A}_0(\tau)\mathrm{e}^{-\frac{pt}{1+\beta}} + \frac{1}{1+\beta}\mathrm{e}^{-\frac{pt}{1+\beta}}\int_0^t \mathrm{e}^{\frac{ps}{1+\beta}}\psi_0(s)\,\mathrm{d}s, \tag{25}$$

where $\mathcal{A}_0(\tau)$ is still an arbitrary function that can be used to avoid secular terms in ϕ_1. Substituting $\phi_0(t,\tau)$ into the $\mathcal{O}(\varepsilon)$-equation results in unbounded terms in ϕ_1 on a time scale of $\mathcal{O}\left(\frac{1}{\varepsilon}\right)$. To eliminate these secular terms, $\mathcal{A}_0(\tau)$ has to be chosen such that ϕ_1 remains bounded for large t. This paper demonstrates this process through examples. First, we use a single sine wave as the IC (as shown in (11)). Given f and g as in (11), we obtain for $\psi_0(t)$ in (24):

$$\psi_0(t) = \begin{cases} 0, & 0 < t < 2\pi, \\ (1-\beta)\cos(t) - p\sin(t), & 2\pi \le t \le 3\pi, \\ 0, & 3\pi < t. \end{cases} \tag{26}$$

First, substitute (26) into (25), and then compute $(\hat{\phi}_0 + \psi(t))^3$. Incorporating this result into the $\mathcal{O}(\varepsilon)$-Eq. (24), we observe that $\hat{\phi}_{0_{t\tau}}$ is the only source for unbounded terms in ϕ_1. Hence, taking $\mathcal{A}_{0_\tau}(\tau) = 0$ ensures ϕ_1 remains bounded for $t = \mathcal{O}\left(\frac{1}{\varepsilon}\right)$. We have to choose $A_0(0,\tau) = 0$ to maintain the continuity of ϕ_0 at zero. With the secular terms eliminated, we can now derive the approximation up to $\mathcal{O}(\varepsilon)$:

$$\phi_a(t-x) = \begin{cases} 0, & 0 < t-x < 2\pi, \\ -\frac{2p}{(1+\beta)^2+p^2}\mathrm{e}^{\frac{p(2\pi-(t-x))}{1+\beta}} + \frac{1-\beta^2-p^2}{(1+\beta)^2+p^2}\sin(t-x) + \frac{2p}{(1+\beta)^2+p^2}\cos(t-x), & 2\pi \le t-x \le 3\pi, \\ -\frac{2p}{(1+\beta)^2+p^2}\left(\mathrm{e}^{\frac{3p\pi}{1+\beta}} + \mathrm{e}^{\frac{2p\pi}{1+\beta}}\right)\mathrm{e}^{-\frac{p(t-x)}{1+\beta}}, & 3\pi < t-x. \end{cases} \tag{27}$$

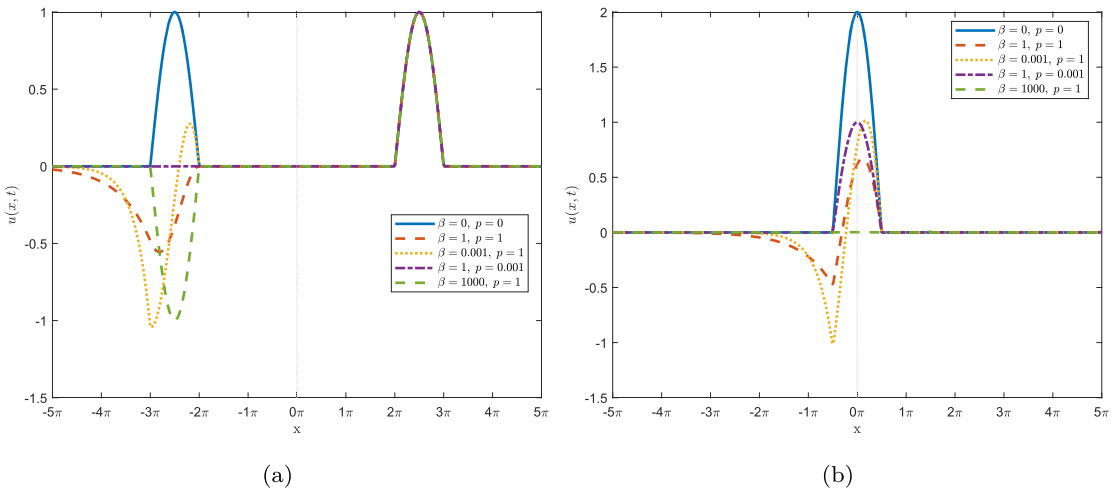

Fig. 4. A single sine wave and its reflections at the boundary for the parameter values $\tilde{m} = 0$ and $\varepsilon \neq 0$, with different values of β and p at time: (a) $t = 0$ and (b) $t = \frac{5}{2}\pi$.

As shown in (27), the elimination of secular terms results in the cancellation of all terms proportional to ε. Consequently, for the ICs given in (11), the cubic nonlinearity in the spring coefficient does not influence our approximation. A similar conclusion was drawn in [36], where the authors considered a quadratic nonlinearity of a spring attached at one end of a string and noted that the nonlinearity also does not affect the behavior of the reflected wave for these ICs (11). This first order approximation ϕ_a is illustrated in Fig. 4a and the interaction at the boundary is illustrated in Fig. 4b. The behavior of the reflected wave is identical to that of the linear BC in Section 4.1.

For the second example, we use continuous sine waves as ICs, given by:

$$\begin{cases} u(x,0) = f(x) = k\sin(\omega x), & x > 0, \\ u_x(x,0) = g(x) = k\omega\cos(\omega x), & x > 0. \end{cases} \tag{28}$$

Applying the same technique as for the previous example, we can find the approximation $\phi_a(t-x)$ as follows.

$$\phi_a(t-x) = -\mathcal{M}e^{-\left(\mathcal{R}\varepsilon+\frac{p}{1+\beta}\right)(t-x)} + \mathcal{M}\cos\left(\omega(t-x)\right) + \mathcal{N}\sin\left(\omega(t-x)\right), \tag{29}$$

with

$$\mathcal{M} = \frac{p(1-\beta)k\omega + p(1+\beta)k\omega^2}{p^2 + (1+\beta)^2\omega^2}, \quad \mathcal{N} = \frac{(1+\beta)(1-\beta)k\omega^2 - p^2k\omega}{p^2 + (1+\beta)^2\omega^2}, \quad \mathcal{R} = \frac{3[\mathcal{M}^2 + (\mathcal{N}+k)^2]}{2(1+\beta)}.$$

The approximation derived in (29) demonstrates that the nonlinearity parameter, ε, influences the frequency shift. Fig. 5 illustrates the wave reflection behavior for $k = 1$ and $\omega = 1$. As shown in Fig. 5a, for $\varepsilon = 0.01$, the reflected wave exhibits a behavior identical to that of a single sine wave. The absence of damping and spring forces in the system results in a symmetric extension of the reflected wave, represented by the blue curve. In contrast, when highly viscous damping is introduced (i.e., a large damping coefficient), the system exhibits minimal motion, resulting in an asymmetric extension of the reflected wave, as shown by the green curve.

Setting the damping and spring coefficients to 1 and 0, respectively, the BC is given by $u_x(0,t) = u_t(0,t) + \varepsilon u^3(0,t)$. Since ε is small, the system exhibits an ideal damping effect (represented by the purple line), which ensures complete absorption of the wave energy at the boundary. The interaction between the spring and damping coefficients attenuates the amplitude of the reflected wave, further demonstrating their combined influence on the behavior of the wave.

Fig. 5b presents the interaction between the incident continuous sine wave and its reflection at $t = \frac{5}{2}\pi$. When the reflection exhibits an even extension, the interaction results in a doubling of the wave amplitude (blue curve). In contrast, an odd extension leads to complete wave cancellation, producing a 'flat' response (green curve). Under ideal damping conditions, there is no reflected wave, highlighting the effectiveness of the damping mechanism in preserving the characteristics of the waves.

4.4. The problem with $\tilde{m} \neq 0$, $\varepsilon \neq 0$, and $\beta = \mathcal{O}(1)$

The objective of this section is to describe the behavior of the string when a nonlinear spring and a mass are integrated into the damping system at the boundary. Hence, we have the following BC for the system (2):

$$u_{tt}(0,t) = u_x(0,t) - pu(0,t) - \varepsilon u^3(0,t) - \beta u_t(0,t). \tag{30}$$

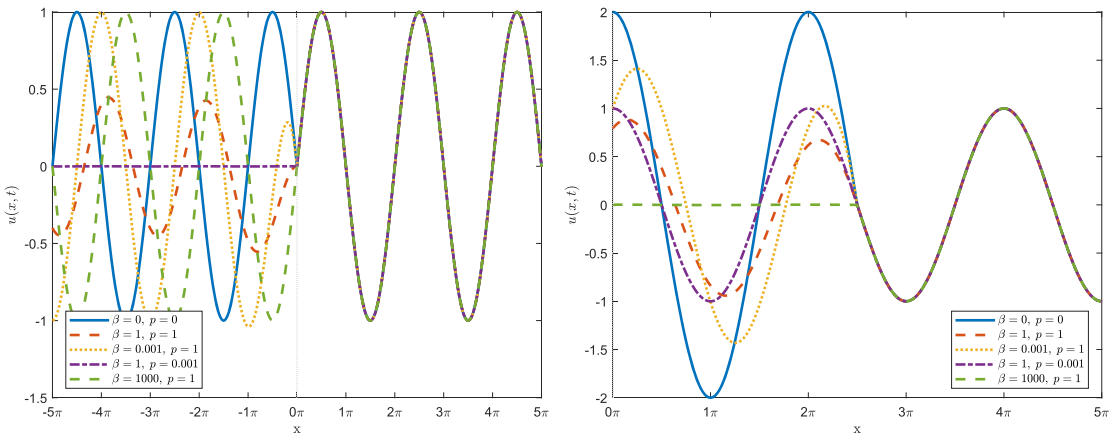

Fig. 5. A continuous sine wave and its reflections at the boundary for the parameter values $\tilde{m} = 0$ and $\varepsilon \neq 0$, with different values of β and p at time: (a) $t = 0$ and (b) $t = \frac{5}{2}\pi$.

Again, using the definitions (6) of $\psi(t)$ and (7) of $\phi(t)$ for the D'Alembert's solution (5), and substituting them into BC (30), we have the following.

$$\phi''(t) + (1+\beta)\phi'(t) + p\phi(t) + \varepsilon\phi^3(t) + 3\varepsilon\phi^2(t)\psi(t) + 3\varepsilon\phi(t)\psi^2(t) = -\psi''(t) + (1-\beta)\psi'(t) - p\psi(t) - \varepsilon\psi^3(t). \tag{31}$$

To approximate the still unknown function ϕ in (31), we use the MSP method, which leads to an asymptotic expansion (23) for $\phi(t)$. Substituting (23) into (31), we obtain the following $\mathcal{O}(1)$ and $\mathcal{O}(\varepsilon)$ problems:

$$\begin{cases} \mathcal{O}(1): & \phi_{0_{tt}} + (1+\beta)\phi_{0_t} + p\phi_0 = -\psi''(t) + (1-\beta)\psi'(t) - p\psi(t), \\ & \phi(0,0) = 0, \\ & \phi_t(0,0) = 0, \\ \mathcal{O}(\varepsilon): & \phi_{1_{tt}} + (1+\beta)\phi_{1_t} + p\phi_1 = -2\phi_{0_{t\tau}} - (1+\beta)\phi_{0_\tau} - \phi_0^3 - 3\phi_0^2\psi(t) - 3\phi_0\psi^2(t) - \psi^3(t), \\ & \phi_1(0,0) = 0, \\ & \phi_{1_t}(0,0) + \phi_{0_\tau}(0,0) = 0. \end{cases} \tag{32}$$

We shall first solve the $\mathcal{O}(1)$-problem in (32). The equation is a non-homogeneous ODE. It has a fundamental set of solutions and a particular solution, that is, $\phi_0 = \phi_{0,f} + \phi_{0,p}$. The fundamental set $\phi_{0,f}$ are solutions to the homogeneous ODE, $\phi_{0_{tt}} + (1+\beta)\phi_{0_t} + p\phi_0 = 0$, and the particular solution $\phi_{0,p}$ is a solution to the non-homogeneous problem, $\phi_{0_{tt}} + (1+\beta)\phi_{0_t} + p\phi_0 = -\psi_{tt}(t) + (1-\beta)\psi_t(t) - p\psi(t)$.

The characteristic equation for our homogeneous equation is $r^2 + (1+\beta)r + p = 0$. This is a regular quadratic equation whose roots are $r_{1,2} = \frac{-(1+\beta)\pm\sqrt{(1+\beta)^2-4p}}{2}$. The nature of the roots depends on the value of $(1+\beta)^2 - 4p$. Again, as in Section 4.3, we have three cases. The solution of the homogeneous ODE is of the form

$$\phi_0(t,\tau) = \mathcal{A}_0(\tau)\phi_{0,f_1}(t) + \mathcal{B}_0(\tau)\phi_{0,f_2}(t), \tag{33}$$

where

$$\begin{cases} \text{case 1:}((1+\beta)^2 > 4p): & \phi_{0,f_1}(t) = \mathrm{e}^{r_1 t}; \quad \phi_{0,f_2}(t) = \mathrm{e}^{r_2 t}, \\ \text{case 2:}((1+\beta)^2 = 4p): & \phi_{0,f_1}(t) = \mathrm{e}^{rt}; \quad \phi_{0,f_2}(t) = t\mathrm{e}^{rt}, \\ \text{case 3:}((1+\beta)^2 < 4p): & \phi_{0,f_1}(t) = \mathrm{e}^{rt}\cos(\mu t); \quad \phi_{0,f_2}(t) = \mathrm{e}^{rt}\sin(\mu t). \end{cases} \tag{34}$$

for

$$r_1 = \frac{-(1+\beta) + \sqrt{(1+\beta)^2 - 4p}}{2}, \quad r_2 = \frac{-(1+\beta) - \sqrt{(1+\beta)^2 - 4p}}{2}, \quad r = \frac{-(1+\beta)}{2}, \quad \text{and} \quad \mu = \frac{\sqrt{4p - (1+\beta)^2}}{2}.$$

To find the particular solution to our problem, we now consider a continuous sine wave (28) as the IC. Given $\psi(t)$ in (6), we then have

$$\begin{cases} \psi(t) = k\sin(\omega t), \\ \psi_t(t) = k\omega\cos(\omega t), \\ \psi_{tt}(t) = -k\omega^2\sin(\omega t). \end{cases} \tag{35}$$

We know that the reflected wave is represented by $\phi(t-x)$ and from (7) and (28), it follows that

$$\phi(0) = \phi_t(0) = 0. \tag{36}$$

A particular solution of the non-homogeneous $\mathcal{O}(1)$-problem (32) is given by:

$$\phi_{0,p}(t) = \frac{2k\omega(p-\omega^2)}{(p-\omega^2)^2+(1+\beta)^2\omega^2}\cos(\omega t) + \frac{-k[(p-\omega^2)^2-(1-\beta^2)\omega^2]}{(p-\omega^2)^2+(1+\beta)^2\omega^2}\sin(\omega t). \tag{37}$$

In the next three subsections, we proceed with a detailed analysis of the reflection of waves for each of the three cases (34) occurring in the $\mathcal{O}(1)$-Eq. (32):

$$\begin{cases} \text{case 1:} & \phi_0(t,\tau) = \mathcal{A}_0(\tau)e^{r_1 t} + \mathcal{B}_0(\tau)e^{r_2 t} + c_1\cos(\omega t) + c_2\sin(\omega t), \\ \text{case 2:} & \phi_0(t,\tau) = \mathcal{A}_0(\tau)e^{rt} + \mathcal{B}_0(\tau)te^{rt} + c_1\cos(\omega t) + c_2\sin(\omega t), \\ \text{case 3:} & \phi_0(t,\tau) = \mathcal{A}_0(\tau)e^{rt}\cos(\mu t) + \mathcal{B}_0(\tau)e^{rt}\sin(\mu t) + c_1\cos(\omega t) + c_2\sin(\omega t), \end{cases} \tag{38}$$

with

$$\begin{cases} c_1 = \frac{2k\omega(p-\omega^2)}{(p-\omega^2)^2+(1+\beta)^2\omega^2}, \\ c_2 = \frac{-k[(p-\omega^2)^2-(1-\beta^2)\omega^2]}{(p-\omega^2)^2+(1+\beta)^2\omega^2}, \end{cases} \tag{39}$$

and where $\mathcal{A}_0(0)$ and $\mathcal{B}_0(0)$ can be determined from (36).

4.4.1. *Case 1:* $(1+\beta)^2 > 4p$

In this case, it follows from (36) and (38) that:

$$\begin{cases} \mathcal{A}_0(0) = \frac{c_1 r_2 - c_2\omega}{r_1 - r_2}, \\ \mathcal{B}_0(0) = \frac{c_2\omega - c_1 r_1}{r_1 - r_2}. \end{cases} \tag{40}$$

To ensure that the approximation remains bounded, on a time-scale of order $\frac{1}{\varepsilon}$, all terms in the RHS of the $\mathcal{O}(\varepsilon)$-equation in (32), which lead to secular terms in ϕ_1 should be eliminated. By equating the coefficient of $e^{r_1 t}$ and the coefficient of $e^{r_2 t}$ to zero, we can eliminate these secular terms (B.1), and find the expressions for $\mathcal{A}_0(\tau)$ and $\mathcal{B}_0(\tau)$, yielding:

$$\begin{cases} \frac{d\mathcal{A}_0(\tau)}{d\tau} = -\frac{\mathcal{G}}{(1+\beta+2r_1)}\mathcal{A}_0(\tau), \\ \frac{d\mathcal{B}_0(\tau)}{d\tau} = -\frac{\mathcal{G}}{(1+\beta+2r_2)}\mathcal{B}_0(\tau), \end{cases} \tag{41}$$

with

$$\mathcal{G} = \frac{3}{2}\left[c_1^2 + (c_2+k)^2\right]. \tag{42}$$

The system (41) can easily be solved. using the ICs given in (40), and we find an approximation $\phi_a(t-x)$ of ϕ in (22):

$$\phi_a(t-x) = \frac{(c_1 r_2 - c_2\omega)}{r_1 - r_2}e^{\left(r_1 - \frac{\mathcal{G}}{r_1 - r_2}\varepsilon\right)(t-x)} + \frac{(c_2\omega - c_1 r_1)}{r_1 - r_2}e^{\left(r_2 - \frac{\mathcal{G}}{r_1 - r_2}\varepsilon\right)(t-x)} + c_1\cos(\omega(t-x)) + c_2\sin(\omega(t-x)), \tag{43}$$

where c_1 and c_2 are given in (39). This approximation (43) is $\mathcal{O}(\varepsilon)$ accurate. Fig. 6 shows how the wave is reflected at the boundary $x=0$ for different values of $\omega, t, \varepsilon, \beta, p$, and with $k=1$.

Similarly to Section 4.1, increasing the damping coefficient drives the boundary response toward an odd reflection of the incident wave, reflecting the dominance of the dissipative impedance in determining reflection symmetry (Fig. 6). Additionally, at low excitation frequencies, the coupled action of damping and spring stiffness alters the effective boundary impedance, resulting in marked amplification or attenuation of the reflected wave amplitude depending on the parameter regime (Fig. 6a). This mechanism is further evidenced by the transition at $t = \frac{5\pi}{2}$, where an undamped, unstiffened boundary yields the classical doubling of the boundary amplitude, while increasing damping progressively suppresses the reflected wave through enhanced energy dissipation (Fig. 6b).

Furthermore, Fig. 6c and d highlight the sensitivity of the reflection on the nonlinearity parameter ε and clearly indicate the complex interplay between nonlinearity, damping, and spring coefficients in defining the temporal and spatial characteristics of wave reflections within the system.

To demonstrate that the method is applicable to all types of ICs, we now consider (11) as ICs. Given $\psi(t)$ in (6), we have

$$\psi(t) = \begin{cases} \sin(t), & 2\pi \le t \le 3\pi, \\ 0, & \text{otherwise.} \end{cases}$$

Then we can find $\psi_t(t)$ and $\psi_{tt}(t)$. A particular solution of the non-homogeneous $\mathcal{O}(1)$-problem in (32) is given by

$$\phi_{0,p}(t) = \begin{cases} \tilde{c}_1\cos(t) + \tilde{c}_2\sin(t), & 2\pi \le t \le 3\pi, \\ 0, & \text{otherwise,} \end{cases} \tag{44}$$

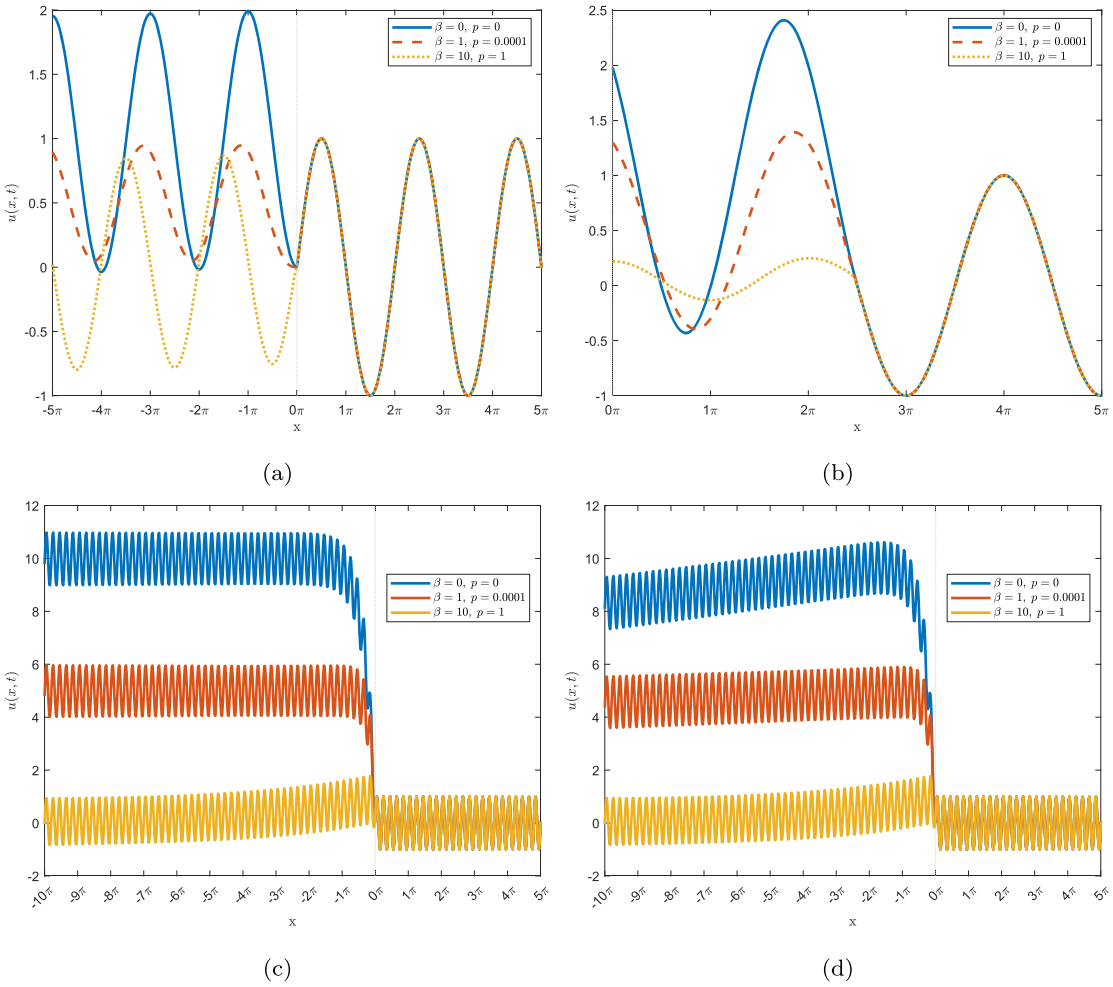

Fig. 6. A continuous sine wave and its reflections at the boundary for the problem $\tilde{m} \neq 0$ and $\varepsilon \neq 0$ for the case $(1+\beta)^2 > 4p$ with different parameters values β, p, and: (a) $\omega = 1$, $\varepsilon = 0.001$, at $t = 0$; (b) $\omega = 1$, $\varepsilon = 0.001$, at $t = \frac{5\pi}{2}$; (c) $\omega = 10$, $\varepsilon = 0.001$, $t = 0$; (d) $\omega = 10$, $\varepsilon = 0.1$, at $t = 0$.

with $\tilde{c}_1 = \dfrac{p-1}{(p-1)^2+(1+\beta)^2}$ and $\tilde{c}_2 = \dfrac{(1-\beta^2)-(p-1)^2}{(p-1)^2+(1+\beta)^2}$. For $t < 2\pi$, the response is zero, consistent with the causality principle and the finite support of the wave packet,

$$\phi_a(t) = 0. \tag{45}$$

During the active interval $2\pi \leq t \leq 3\pi$, we take

$$\phi_a(t) = \mathcal{A}_0 e^{\zeta_1(t-2\pi)} + \mathcal{B}_0 e^{\zeta_2(t-2\pi)} + c_1 \cos\big(\omega(t-2\pi)\big) + c_2 \sin\big(\omega(t-2\pi)\big), \tag{46}$$

with $\zeta_i = r_i - \dfrac{\mathcal{G}}{r_1 - r_2}\varepsilon$. After the reflected wave leaves the boundary at $t = 3\pi$, the forcing vanishes, and (34) reduces to the homogeneous equation. Hence, the solution for $t > 3\pi$ is purely a free decay,

$$\phi_a(t) = D_1 e^{\zeta_1(t-3\pi)} + D_2 e^{\zeta_2(t-3\pi)}. \tag{47}$$

The constants D_1, D_2 are determined by the continuity of ϕ and ϕ_t at $t = 3\pi$. Denoting $\Phi := \phi(3\pi^-)$ and $\Phi' := \phi_t(3\pi^-)$, we obtain the linear system

$$\begin{cases} D_1 + D_2 = \Phi, \\ \zeta_1 D_1 + \zeta_2 D_2 = \Phi', \end{cases} \tag{48}$$

which yields the explicit matching coefficients

$$\begin{cases} D_1 = \dfrac{\Phi' - \zeta_2 \Phi}{\zeta_1 - \zeta_2}, \\ D_2 = \dfrac{\zeta_1 \Phi - \Phi'}{\zeta_1 - \zeta_2}. \end{cases} \tag{49}$$

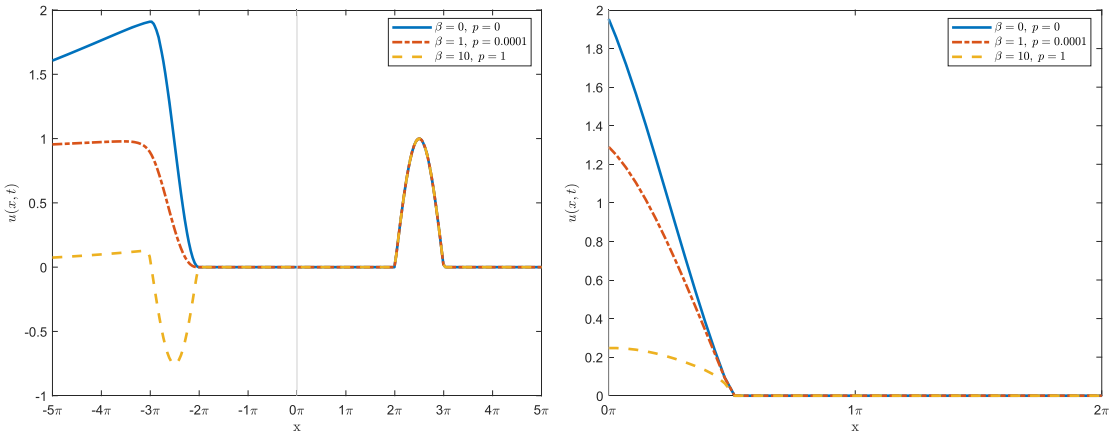

Fig. 7. A single sine wave and its reflections at the boundary for the problem $\tilde{m} \neq 0$ and $\varepsilon = 0.01$ for the case $(1+\beta)^2 > 4p$ with different parameters values β and p at time: (a) $t = 0$, (b) $t = \frac{5\pi}{2}$.

Collecting (45)–(47), the approximation of $\phi(\hat{t})$, with $\hat{t} = (t - x)$, is given by

$$\phi_a(\hat{t}) = \begin{cases} 0, & \hat{t} < 2\pi, \\ \mathcal{A}_0 e^{\zeta_1(\hat{t}-2\pi)} + \mathcal{B}_0 e^{\zeta_2(\hat{t}-2\pi)} + \tilde{c}_1 \cos\big(\omega(\hat{t}-2\pi)\big) + \tilde{c}_2 \sin\big(\omega(\hat{t}-2\pi)\big), & 2\pi \leq \hat{t} \leq 3\pi, \\ D_1 e^{\zeta_1(\hat{t}-3\pi)} + D_2 e^{\zeta_2(\hat{t}-3\pi)}, & \hat{t} > 3\pi, \end{cases} \tag{50}$$

where $\mathcal{A}_0, \mathcal{B}_0$ are given by (40) and D_1, D_2 by (49).

As shown in Fig. 7, the reflected wave exhibits a behavior identical to that obtained for a continuous sine ICs. However, under a single sine excitation, the nonlinear boundary response produces a noticeably longer trailing tail than the linear case presented in (4.2). This observation indicates that the nonlinear boundary influence extends beyond the primary reflection, leading to a prolonged response in the reflected wave.

4.4.2. *Case 2:* $(1+\beta)^2 = 4p$

In this case of coinciding eigenvalues, the elimination of resonance terms will not result in an ODE system to determine $\mathcal{A}_0(\tau)$ and $\mathcal{B}_0(\tau)$ in (38). This contradicts [37], which reported an ODE system for a case similar to $\frac{d\mathcal{A}_0(\tau)}{d\tau} = 0$. Hence, for this case, we use the naive perturbation method to approximate $\phi_a(t-x)$ in (22). To do this, we first make sure that the approximation is bounded. Let

$$\phi(t) = \phi_0 + \varepsilon\phi_1 + \varepsilon^2\phi_2 + \dots \tag{51}$$

For the critically damped case, the solution for $\phi(t)$ in (31) can be approximated with

$$\phi(t) \sim \phi_0(t) + \varepsilon\phi_1(t). \tag{52}$$

This gives secular terms in the form $\varepsilon(te^{rt}, \dots, t^3e^{rt})$. We can see that these terms are bounded. Let

$$\mathcal{F} = t^n e^{rt},$$
$$\mathcal{F}' = (n + rt)t^{n-1}e^{rt},$$

has a maximum at $t = -\frac{n}{r}$, which is given by

$$\mathcal{F} = \left(-\frac{n}{r}\right)^n e^{-n} = \left(-\frac{n}{er}\right)^n. \tag{53}$$

Given that $r \leq -\frac{1+\beta}{2}$, the solution ϕ_1 in (51) has a maximum. We also see that $te^{rt}, \dots, t^3e^{rt}$ is $\mathcal{O}(\varepsilon)$, which means small. Since ϕ_1 is bounded and small, we argue that the solution will not blow up. Therefore, our solution can be well-approximated with the solution up to $\mathcal{O}(\varepsilon)$-problem.

It follows from (31) and (51), we obtain $\mathcal{O}(1)-$ and $\mathcal{O}(\varepsilon)-$problems:

$$\begin{cases} \mathcal{O}(1): & \phi_0'' + (1+\beta)\phi_0' + p\phi_0 = -\psi'' + (1-\beta)\psi' - p\psi, \\ & \phi(0) = 0, \quad \phi'(0) = 0, \end{cases}$$
$$\begin{cases} \mathcal{O}(\varepsilon): & \phi_1'' + (1+\beta)\phi_1' + p\phi_1 = -\phi_0^3 - 3\phi_0^2\psi - 3\phi_0\psi^2 - \psi^3, \\ & \phi_1(0) = 0, \quad \phi_1'(0) = 0. \end{cases} \tag{54}$$

It follows from (35) and (36) that the solution of the ODE in the $\mathcal{O}(1)$-problem (54) is

$$\phi_0(t) = \mathcal{A}_0 e^{rt} + \mathcal{B}_0 t e^{rt} + c_1 \cos(\omega t) + c_2 \sin(\omega t), \tag{55}$$

with

$$\begin{cases} \mathcal{A}_0 = -c_1, \\ \mathcal{B}_0 = r c_1 - c_2 \omega. \end{cases} \tag{56}$$

Next, we consider the $\mathcal{O}(\varepsilon)$-problem in (54). The solution of the $\mathcal{O}(\varepsilon)$-problem in (54) is

$$\begin{aligned} \phi_1(t) = {} & (\mathcal{A}_1 + \mathcal{B}_1 t) e^{rt} + \phi_{1,p}(t) + e^{3rt} \sum_{m=0}^{3} U_m t^m + e^{2rt} \sum_{m=0}^{2} \big(\upsilon_m \cos(\omega t) + \nu_m \sin(\omega t)\big) t^m + \mathcal{G} t^2 e^{rt} \Big(-\tfrac{1}{2}\mathcal{A}_0 - \tfrac{1}{6}\mathcal{B}_0 t\Big) \\ & + e^{rt} \sum_{m=0}^{1} \big(\hat{\upsilon}_m \cos(2\omega t) + \hat{\nu}_m \sin(2\omega t)\big) t^m, \end{aligned} \tag{57}$$

where $\mathcal{A}_0, \mathcal{B}_0$, and $\mathcal{G}$ are given in (56) and (42). The complete extension of the other variables can be seen in Appendix B.2.

Using the results in (55) and (57), it follows from (52) that the approximation ϕ_a for ϕ in (22) is given by

$$\begin{aligned} \phi_a(t-x) = {} & -c_1 e^{r(t-x)} + (r c_1 - c_2 \omega)(t-x) e^{r(t-x)} + c_1 \cos(\omega(t-x)) + c_2 \sin(\omega(t-x)) \\ & + \varepsilon \Big[(\mathcal{A}_1 + \mathcal{B}_1 (t-x)) e^{r(t-x)} + \phi_{1,p}((t-x)) + e^{3r(t-x)} \sum_{m=0}^{3} U_m (t-x)^m \\ & + e^{2r(t-x)} \sum_{m=0}^{2} \big(\upsilon_m \cos(\omega(t-x)) + \nu_m \sin(\omega(t-x))\big)(t-x)^m + \mathcal{G}(t-x)^2 e^{r(t-x)} \Big(-\tfrac{1}{2}\mathcal{A}_0 - \tfrac{1}{6}\mathcal{B}_0 (t-x)\Big) \\ & + e^{r(t-x)} \sum_{m=0}^{1} \big(\hat{\upsilon}_m \cos(2\omega(t-x)) + \hat{\nu}_m \sin(2\omega(t-x))\big)(t-x)^m \Big], \end{aligned} \tag{58}$$

where c_1 and c_2 are given by (39). As shown in (58), the cubic nonlinearity affects the solution. The behavior of the reflected wave can be seen in Fig. 8. Again, in this visualization, we take $k = 1$.

First, in this critically damped case, Fig. 8 shows that the relative values of the damping and spring coefficients determine whether the wave reflection exhibits an even or odd extension. This dependence suggests a direct relationship between the coefficient ratios and the symmetry properties of the reflected wave. Consequently, the wave transition at the boundary is depicted in Fig. 8b. The interaction between the incoming and reflected waves results in varying wave amplitudes, determined by the reflected wave's behavior. Specifically, a low-damping configuration leads to an amplified wave amplitude (blue line) at certain times, whereas a high-damping configuration achieves complete absorption with an amplitude matching the incoming wave (red line). Conversely, when the reflection exhibits an odd extension, the resulting wave amplitude is reduced (yellow line) for a certain time.

Second, for an arbitrary frequency ω, the reflected wave decays more rapidly as the damping coefficient increases, convergent to the frequency of the incident wave in a shorter time frame (as illustrated in Fig. 8c). This accelerated decay under critical damping conditions highlights how efficiently energy dissipation aligns the reflected and incoming wave frequencies [38,39].

Third, in this particular case with specific incoming wave form (28), complete energy absorption for low-frequency oscillations, specifically for $\omega \approx 1$, has been identified when both the damping coefficient β and the linear spring coefficient p are equal to 1 (red line in Fig. 8). Under these conditions-$\omega = 1, \beta = 1$, and $p = 1$-the displacement u is approximately zero for the region where $x - t < 0$, indicating that the wave reflections are effectively minimized. However, it is important to note that this does not imply the existence of an ideal damping for all scenarios, as the system is subject to specific ICs and constraints (4). These conditions dictate the interplay among damping, reflection, and amplitude, highlighting the need for tailor-made configurations for specific scenarios. This finding is in line with the analysis of [40], which emphasizes the strong dependence of vibrating systems on ICs to determine optimal damping. This also suggests the potential to adjust damping parameters for varying frequencies, showcasing the system's tunability.

We also consider the single sine wave (11) as the ICs. As in the overdamped case, the excitation is active only for $2\pi \le t - x \le 3\pi$, and the approximation ϕ_a is applied locally in time. The boundary response is therefore defined as

$$\phi(t-x) = \begin{cases} 0, & t - x < 2\pi, \\ \phi_a(t - x - 2\pi), & 2\pi \le t - x \le 3\pi, \\ \big(\mathcal{D}_1 + \mathcal{D}_2 (t - x - 3\pi)\big) e^{r(t-x-3\pi)}, & t - x > 3\pi, \end{cases} \tag{59}$$

where $\phi_a(t)$ for $2\pi \le t \le 3\pi$ is given by (58). The constants $\mathcal{D}_1$ and $\mathcal{D}_2$ are obtained by enforcing the continuity of ϕ and ϕ_t in $t - x = 3\pi$, yielding $\mathcal{D}_1 = \Phi, \mathcal{D}_2 = \Phi' - r\Phi$, with $\Phi = \phi(3\pi^-)$, $\Phi' = \phi_t(3\pi^-)$, and $r = -\frac{1+\beta}{2}$.

Fig. 9 illustrates the propagation of a single sine wave incident from the positive x-direction and the reflected wave generated at the left boundary. The interaction between the incoming and reflected waves at the boundary is clearly observed. As in the previous example, the behavior of the reflected wave is governed by the relative values of p and β. At $t = \frac{5\pi}{2}$, a boundary close to a free end leads to an increased amplitude of the combined wave field (blue line in Fig. 7b), while a stiffer boundary results in a strongly reduced amplitude and an almost flat profile (yellow line in Fig. 7b).

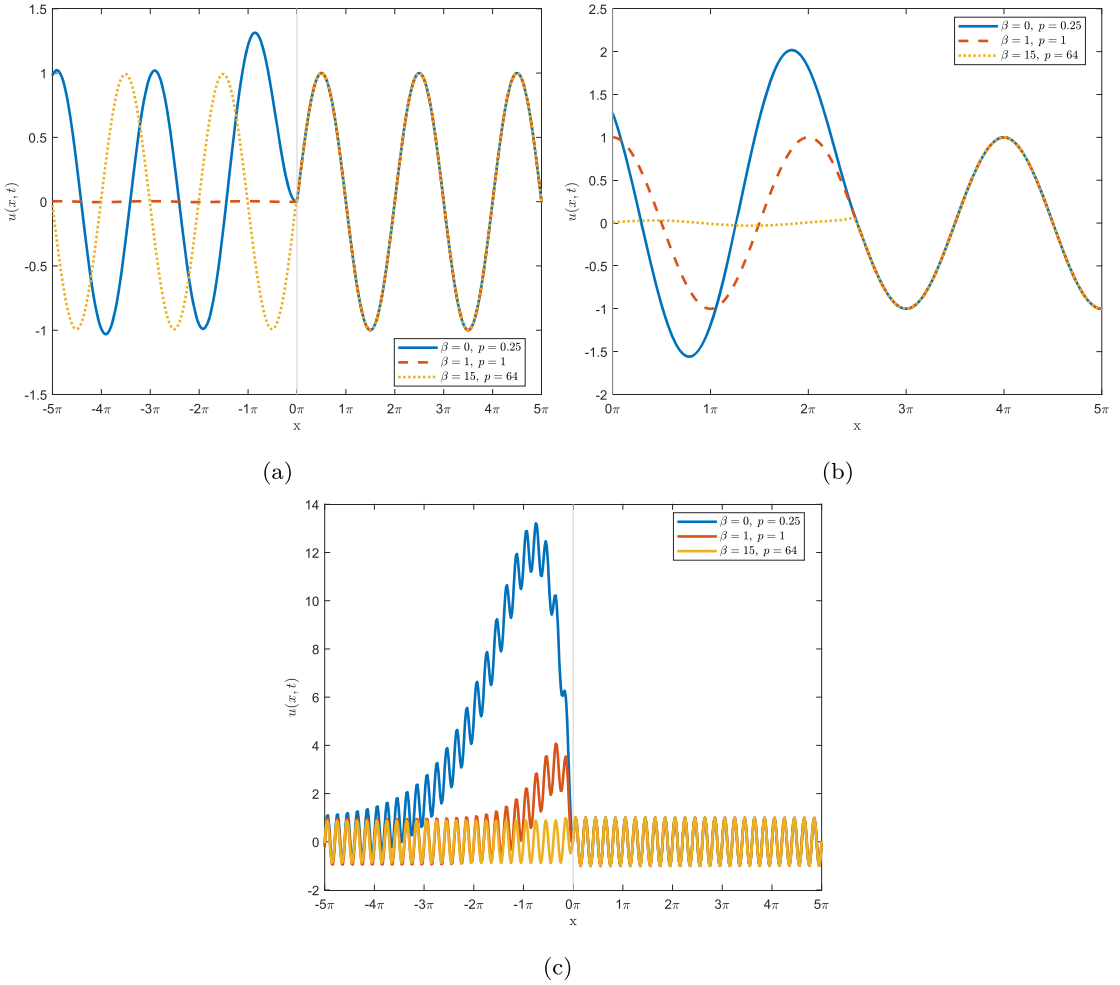

Fig. 8. A continuous sine wave and its reflections at the boundary for the problem with $\tilde{m} \neq 0$, $\varepsilon \neq 0$, and $(1+\beta)^2 = 4p$ for different parameters values β, p, and: (a) $\omega = 1$, $\varepsilon = 0.01$, at $t = 0$; (b) $\omega = 1$, $\varepsilon = 0.01$, at $t = \frac{5\pi}{2}$; (c) $\omega = 10$, $\varepsilon = 0.001$, at $t = 0$.

4.4.3. *Case 3:* $(1+\beta)^2 < 4p$

In this case, it follows from (36) and (38) that the ICs are given by:

$$\begin{cases} \mathcal{A}_0(0) = -c_1, \\ \mathcal{B}_0(0) = \frac{rc_1 - \omega c_2}{\mu}. \end{cases} \tag{60}$$

Considering the $\mathcal{O}(\varepsilon)$-problem in (32), we should find the secular terms in ϕ_1 and equate the coefficients of $e^{rt}\cos(\mu t)$ and $e^{rt}\sin(\mu t)$ to zero (see Appendix B.3). We then find the following system

$$\begin{cases} \frac{d\mathcal{A}_0(\tau)}{d\tau} = \frac{1}{2\mu}\mathcal{G}\mathcal{B}_0(\tau), \\ \frac{d\mathcal{B}_0(\tau)}{d\tau} = -\frac{1}{2\mu}\mathcal{G}\mathcal{A}_0(\tau), \end{cases} \tag{61}$$

when $\mathcal{G}$ is given by (42). We solve system (61) and obtain for $\phi_a(x-t)$ in (22) as follows

$$\begin{aligned} \phi_a(t-x) = &-c_1 e^{r(t-x)}\cos\left(\left(\frac{\mathcal{G}}{2\mu}\varepsilon + \mu\right)(t-x)\right) + \frac{rc_1 - \omega c_2}{\mu}e^{r(t-x)}\sin\left(\left(\frac{\mathcal{G}}{2\mu}\varepsilon + \mu\right)(t-x)\right) \\ &+ c_1\cos(\omega(t-x)) + c_2\sin(\omega(t-x)). \end{aligned} \tag{62}$$

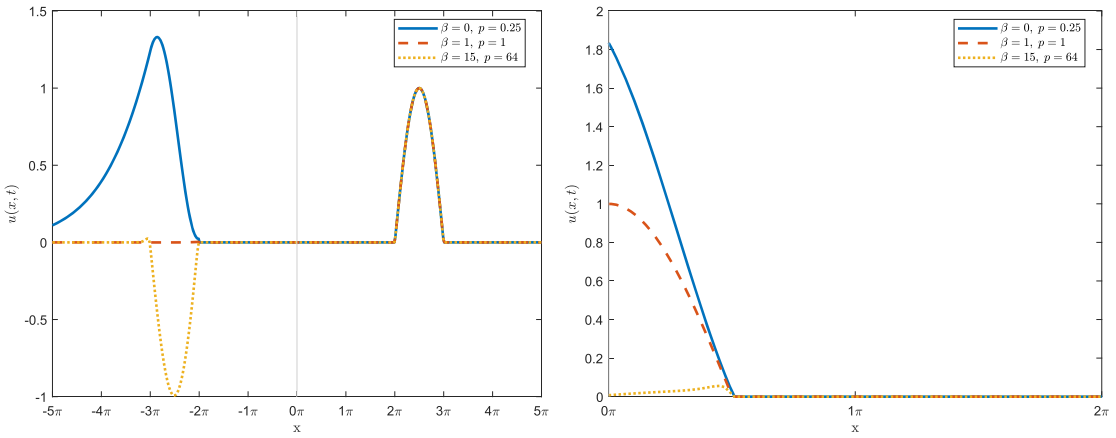

Fig. 9. A single sine wave and its reflections at the boundary for the problem $\tilde{m} \neq 0$ and $\varepsilon = 0.01$ for the case $(1+\beta)^2 = 4p$ with different parameters values β and p at time: (a) $t = 0$, (b) $t = \frac{5\pi}{2}$.

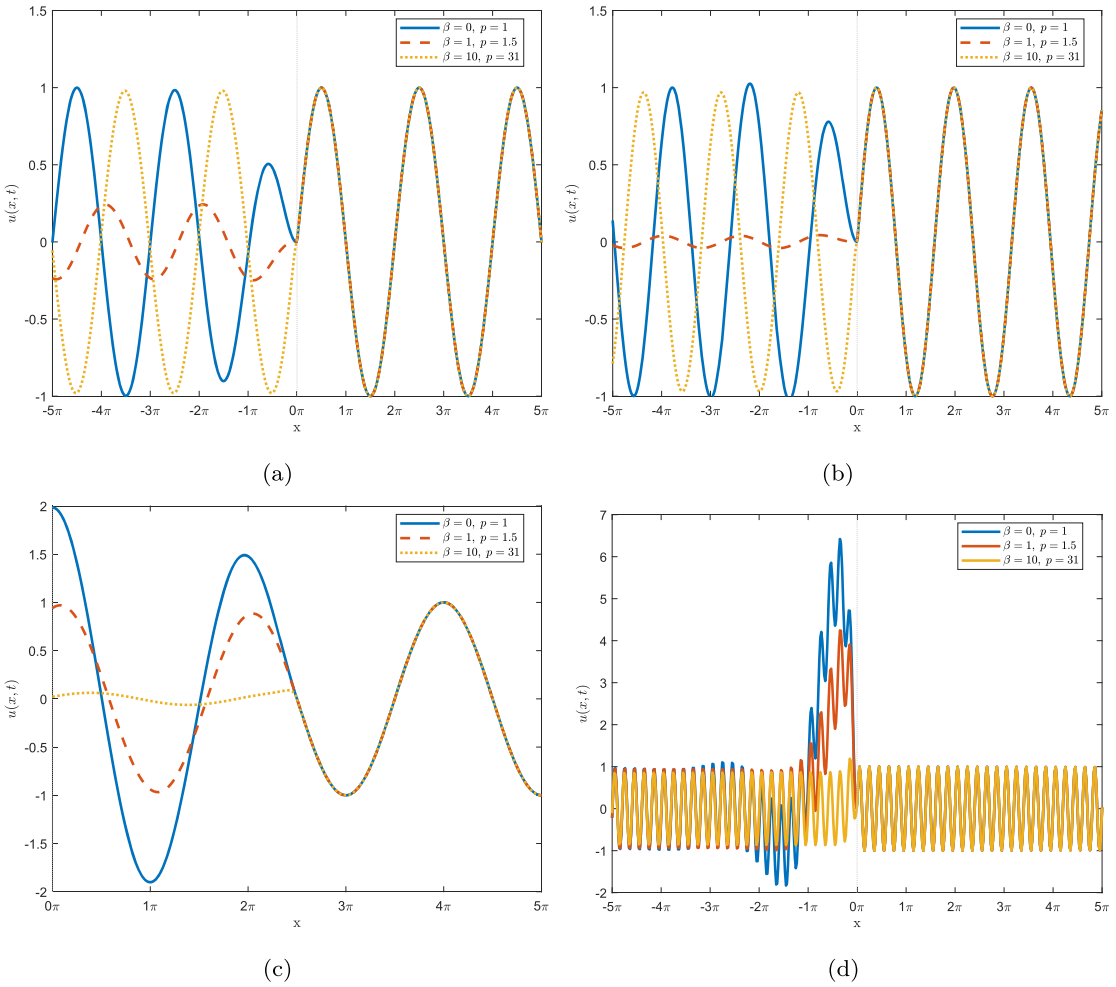

Fig. 10. A continuous sine wave and its reflections at the boundary for the problem with $\tilde{m} \neq 0$, $\varepsilon = 0.01$, and $(1+\beta)^2 < 4p$ for different parameters values β, p, and: (a) $\omega = 1$ at $t = 0$; (b) $\omega = 1.265$ at $t = 0$; (c) $\omega = 1$ at $t = \frac{5\pi}{2}$; (d) $\omega = 10$ at $t = 0$.

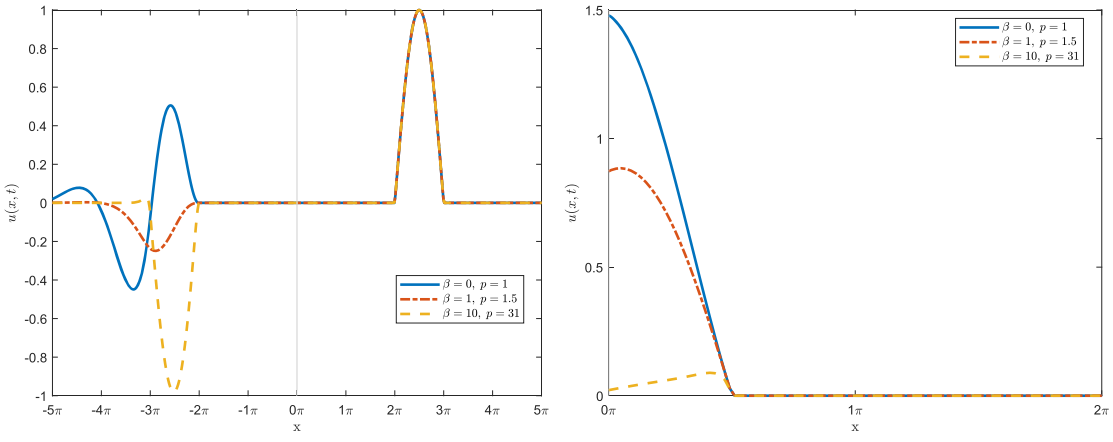

Fig. 11. A single sine wave and its reflections at the boundary for the problem $\tilde{m} \neq 0$ and $\varepsilon = 0.01$ for the case $(1+\beta)^2 < 4p$ with different parameters values β and p at time: (a) $t = 0$, (b) $t = \frac{5\pi}{2}$.

As shown in (62), the nonlinearity parameter significantly influences the modulation of the frequency of the reflected wave. This impact is visually captured in Fig. 10. The results show clearly that both damping and spring coefficients play crucial roles in shaping the waveform, as shown in Fig. 10a. Furthermore, Fig. 10a and b demonstrate that variations in the incoming frequency ω lead to pronounced changes in the amplitude of the reflected wave. This relationship arises from the solution's intricate dependency on the parameters ω, β, p, and ε, which consistently modulate the system's response across all observed cases. In this case a near-optimal configuration can be identified, where $\omega = 1.265, \beta = 1, p = 1.5$, and $\varepsilon = 0.01$, for which a minimized reflection amplitude of approximately 0.04 can be observed. This observation implies the feasibility of identifying highly efficient damping configurations that minimize reflection amplitudes under varying system conditions.

We also illustrate the transition of the wave at $t = \frac{5\pi}{2}$ (see Fig. 10c). The result is consistent with the previous cases. Wave amplitudes vary based on the reflected wave's behavior. Low damping amplifies the wave (blue line) at certain times, specific damping achieves near-complete absorption, matching the incoming wave (red line), and odd-extension reflections reduce amplitude (yellow line) at certain times.

Furthermore, similar to previous cases, the reflected wave returns to its incident frequency more rapidly as the damping and spring coefficients increase, as illustrated in Fig. 10d. This faster convergence highlights the efficiency of energy dissipation, in which the system quickly stabilizes and aligns the reflected wave frequency with that of the incoming wave. By contrast, systems with smaller damping coefficients exhibit prolonged oscillatory behavior before achieving frequency matching, underscoring the crucial role of damping in governing wave decay and frequency alignment.

We also consider the single sine wave (11) as the ICs. As in the overdamped case, the excitation is active only for $2\pi \leq t - x \leq 3\pi$, and the underdamped approximation ϕ_a is applied locally in time. The boundary response is therefore defined as

$$\phi(t-x) = \begin{cases} 0, & t - x < 2\pi, \\ \phi_a(t - x - 2\pi), & 2\pi \leq t - x \leq 3\pi, \\ e^{r(t-x-3\pi)}\left[D_1 \cos(\xi(t - x - 3\pi)) + D_2 \sin(\xi(t - x - 3\pi))\right], & t - x > 3\pi, \end{cases} \tag{63}$$

where $\phi_a(t)$ for $2\pi \leq t \leq 3\pi$ is given by (58), and $\xi = \mu + \frac{\mathcal{G}}{2\mu}\varepsilon$. The constants D_1 and D_2 are obtained by enforcing the continuity of ϕ and ϕ_t at $t - x = 3\pi$, yielding $D_1 = \Phi, D_2 = \frac{\Phi' - r\Phi}{\xi}$, with $\Phi = \phi(3\pi^-)$ and $\Phi' = \phi_t(3\pi^-)$.

Fig. 11 illustrates the reflected wave behavior for different combinations of p and β. As in the previous example with the continuous sine wave ICs (28), the same qualitative conclusions can be drawn regarding the reflected wave response. In particular, lower effective damping leads to a more pronounced reflected response, while higher damping suppresses the reflection more rapidly.

4.5. *The problem of $\tilde{m} \neq 0$, $\varepsilon \neq 0$, and $\beta = \mathcal{O}(\varepsilon)$*

In Section 4.4 we considered relatively strong damping, that is, $\beta = \mathcal{O}(1)$. From a physical point of view, the damper in the system can have the same order as the nonlinearity parameter ε. Therefore, we will analyze case $\beta = \mathcal{O}(\varepsilon)$ to match the order of the nonlinear damping coefficient. This change in order implies weak boundary damping. Therefore, it leads to different dynamics in terms of the behavior of the reflected waves. A similar problem has been studied in [37]. However, in this study, we extend the study by considering the same order but not necessarily the same value for the nonlinear spring and damper coefficients.

Let $\beta = \varepsilon\hat{\beta}$, then the BC in (2) becomes:

$$u_{tt}(0,t) = u_x(0,t) - pu(0,t) - \varepsilon u^3(0,t) - \varepsilon\hat{\beta}u_t(0,t). \tag{64}$$

Hence, from (2) and (3), it follows from the ICs and the BC that:

$$f_{xx}(0) = f_x(0) - pf(0) - \varepsilon f^3(0) - \varepsilon\hat{\beta}g(0). \tag{65}$$

Using the definition (6) for $\psi(t)$ and (7) for $\phi(t)$ in the D'Alembert's formula (Eq. 5) and substituting this formula into the BC, we obtain:

$$\phi''(t) + \phi'(t) + \varepsilon\hat{\beta}\phi_t(t) + p\phi(t) + \varepsilon\phi^3(t) + 3\varepsilon\phi^2(t)\psi(t) + 3\varepsilon\phi(t)\psi^2(t) = -\psi''(t) + \psi'(t) - \varepsilon\hat{\beta}\psi_t(t) - p\psi(t) - \varepsilon\psi^3(t). \tag{66}$$

Assuming that the ICs (28 are given, and using (35)) and MSP method to obtain an asymptotic expansion for $\phi(t)$, where the slow time scale, $\tau = \varepsilon t$, we obtain as before an $\mathcal{O}(1)-$ and an $\mathcal{O}(\varepsilon)-$problems.

$$\begin{cases} \mathcal{O}(1): & \phi_{0_{tt}} + \phi_{0_t} + p\phi_0 = -\psi''(t) + \psi'(t) - p\psi(t) = \psi_0(t), \\ & \phi(0) = 0, \\ & \phi_t(0) = 0. \end{cases}$$

$$\begin{cases} O(\varepsilon): & \phi_{1_{tt}} + \phi_{1_t} + p\phi_1 = -2\phi_{0_{t\tau}} - \phi_{0_\tau} - \hat{\beta}\phi_{0_t} - \phi_0^3 - 3\phi_0^2\psi(t) \\ & -3\phi_0\psi^2(t) - \hat{\beta}\psi_t(t) - \psi^3(t), \\ & \phi_1(0) = 0, \\ & \phi_{1_t}(0) + \phi_{0_\tau}(0) = 0, \end{cases} \tag{67}$$

where $\psi_0(t) = (k\omega^2 - pk)\sin(\omega t) + k\omega\cos(\omega t)$.

The solution of the $\mathcal{O}(1)$-problem (67) is given by

$$\phi_0(t,\tau) = \mathcal{A}_0(\tau)\phi_{0,f_1}(t) + \mathcal{B}_0(\tau)\phi_{0,f_2}(t) + c_3\cos(\omega t) + c_4\sin(\omega t), \tag{68}$$

where $\mathcal{A}_0(\tau)$ and $\mathcal{B}_0(\tau)$ are arbitrary functions, which will be used to avoid secular terms in ϕ_1, where ϕ_{0,f_1} and ϕ_{0,f_2} are given in (70), and where $c_3\cos(\omega t) + c_4\sin(\omega t)$ is the particular solution, and c_3 and c_4 is given by

$$\begin{cases} c_3 = \frac{2k\omega(p-\omega^2)}{(p-\omega^2)^2+\omega^2}, \\ c_4 = \frac{-k[(p-\omega^2)^2-\omega^2]}{(p-\omega^2)^2+\omega^2}. \end{cases} \tag{69}$$

The characteristic equation of the $\mathcal{O}(1)$-problem (67) has roots $r_{1,2} = \frac{-1\pm\sqrt{1-4p}}{2}$. The nature of the roots depends on the value of $\sqrt{1-4p}$. Hence, our approximation of the solution for each case yields:

$$\begin{cases} (p < \frac{1}{4}): & \phi_0(t,\tau) = \mathcal{A}_0(\tau)e^{r_1 t} + \mathcal{B}_0(\tau)e^{r_2 t} + c_3\cos(\omega t) + c_4\sin(\omega t), \\ (p = \frac{1}{4}): & \phi_0(t,\tau) = \mathcal{A}_0(\tau)e^{rt} + \mathcal{B}_0(\tau)te^{rt} + c_3\cos(\omega t) + c_4\sin(\omega t), \\ (p > \frac{1}{4}): & \phi_0(t,\tau) = \mathcal{A}_0(\tau)e^{rt}\cos(\mu t) + \mathcal{B}_0(\tau)e^{rt}\sin(\mu t) + c_3\cos(\omega t) + c_4\sin(\omega t), \end{cases} \tag{70}$$

where $r_1 = \frac{-1+\sqrt{1-4p}}{2}; r_2 = \frac{-1-\sqrt{1-4p}}{2}; r = -\frac{1}{2}$; and $\mu = \frac{\sqrt{4p-1}}{2}$. Notice that these cases do not depend on $\hat{\beta}$ since now the damping coefficient is in the $\mathcal{O}(\varepsilon)$-problem (67).

4.5.1. Case 1: $p < \frac{1}{4}$ and $\beta = \mathcal{O}(\varepsilon)$

In this case, it follows from (36) and (70) that:

$$\begin{cases} \mathcal{A}_0(0) = \frac{c_3 r_2 - c_4\omega}{r_1 - r_2}, \\ \mathcal{B}_0(0) = \frac{c_4\omega - c_3 r_1}{r_1 - r_2} \end{cases} \tag{71}$$

To eliminate terms that lead to secular terms in ϕ_1 (see Appendix B.4), it follows from (67) that $\mathcal{A}_0(\tau)$ and $\mathcal{B}(\tau)$ must satisfy:

$$\begin{cases} \frac{d\mathcal{A}_0(\tau)}{d\tau} = -\frac{\hat{\beta}r_1 + \mathcal{H}}{1+2r_1}\mathcal{A}_0(\tau), \\ \frac{d\mathcal{B}_0(\tau)}{d\tau} = -\frac{\hat{\beta}r_2 + \mathcal{H}}{1+2r_2}\mathcal{B}_0(\tau), \end{cases} \tag{72}$$

where

$$\mathcal{H} = \frac{3}{2}\left[c_3^2 + (c_4 + k)^2\right]. \tag{73}$$

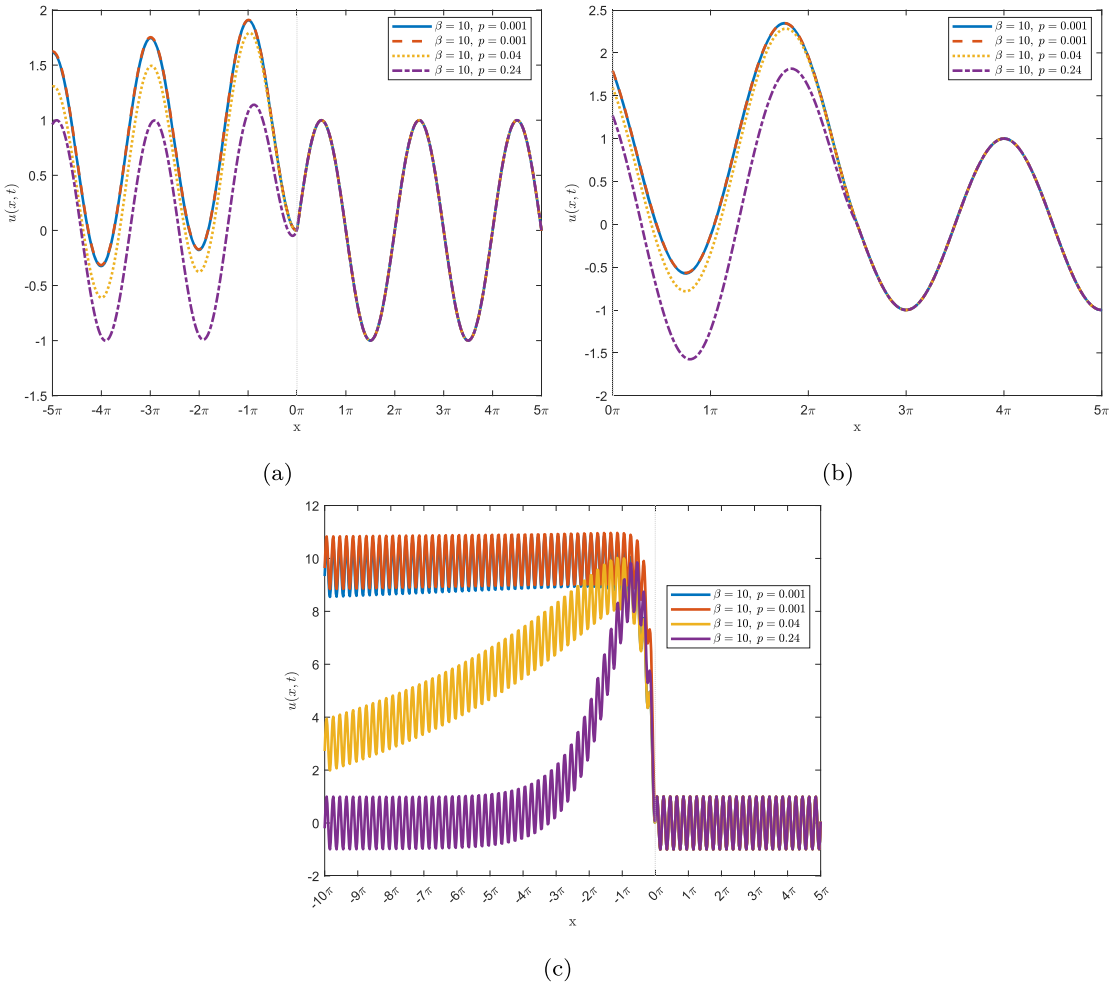

Fig. 12. A continuous sine wave and its reflections at the boundary for the problem $\tilde{m} \neq 0$ and $\varepsilon = 0.01$ for the case $\hat{\beta} = \mathcal{O}(\varepsilon)$, $p < \frac{1}{4}$, and: (a) $\omega = 1$ at $t = 0$; (b) $\omega = 1$ at $t = \frac{5\pi}{2}$; (c) $\omega = 10$ at $t = 0$.

The solution of (72) is given by

$$\begin{cases} \mathcal{A}_0(\tau) = \frac{c_3 r_2 - c_4 \omega}{r_1 - r_2} \mathrm{e}^{-\frac{\hat{\beta} r_1 + \mathcal{H}}{1+2r_1}\tau}, \\ \mathcal{B}_0(\tau) = \frac{c_4 \omega - c_3 r_1}{r_1 - r_2} \mathrm{e}^{-\frac{\hat{\beta} r_2 + \mathcal{H}}{1+2r_2}\tau}, \end{cases} \tag{74}$$

where $\mathcal{H}$ is given by (73). Substituting (74) into $\phi_0(t-x)$, we have as an approximation ϕ_a of ϕ:

$$\phi_a(t-x) = \frac{c_3 r_2 - c_4 \omega}{r_1 - r_2} \mathrm{e}^{\left(r_1 - \frac{\hat{\beta} r_1 + \mathcal{H}}{1+2r_1}\varepsilon\right)(t-x)} + \frac{c_4 \omega - c_3 r_1}{r_1 - r_2} \mathrm{e}^{\left(r_2 - \frac{\hat{\beta} r_2 + \mathcal{H}}{1+2r_2}\varepsilon\right)(t-x)} + c_3 \cos(\omega(t-x)) + c_4 \sin(\omega(t-x)). \tag{75}$$

To illustrate how the wave is reflected at the boundary, we refer to Fig. 12 for $k = 1$. The nonlinearity significantly influences the modulation of the amplitude within the system. In particular, the solution provided in (75) contains exponential terms that incorporate the nonlinearity parameter ε and the damping coefficient $\hat{\beta}$. This is consistent with the fact that now $\hat{\beta} = \mathcal{O}(\varepsilon)$. Consequently, the damping effect in this system is intrinsically linked to nonlinearity ε. In this context, selecting a smaller value of ε minimizes the influence of the damping (weak damping), effectively reducing its impact regardless of the magnitude of the damping coefficient. This effect is illustrated in Fig. 12a and c, where we take low frequency ($\omega = 1$) and high frequency ($\omega = 10$) with $\varepsilon = 0.01$, showing a small damping contribution (the blue and red lines coincide). Furthermore, due to the inherent restrictions imposed by the parameter constraints $p < \frac{1}{4}$ and $0 \leq \varepsilon \ll 1$, the reflected wave will consistently exhibit a relatively even extension to the incident wave. Additionally, we illustrate the wave transition at the boundary at $t = \frac{5\pi}{2}$, where the even extension of the reflection amplifies its interaction with the incoming wave, resulting in a higher amplitude (Fig. 12b).

4.5.2. Case 2: $p = \frac{1}{4}$ and $\beta = \mathcal{O}(\varepsilon)$

In this case, we use the same approach as in Section 4.4.2. Substituting (51) into (66) and equating the coefficients of ε produces $\mathcal{O}(1)-$ and $\mathcal{O}(\varepsilon)-$problems:

$$\begin{cases} \mathcal{O}(1): & \phi_0'' + \phi_0' + p\phi_0 = -\psi'' + \psi' - p\psi, \\ & \phi(0) = 0, \quad \phi'(0) = 0, \\ \mathcal{O}(\varepsilon): & \phi_1'' + \phi_1' + p\phi_1 = -\hat{\beta}\phi_0' - \phi_0^3 - 3\phi_0^2\psi - 3\phi_0\psi^2 - \psi^3, \\ & \phi_1(0) = 0, \quad \phi_1'(0) = 0. \end{cases} \tag{76}$$

It follows from (35) and (36) that the solution of the ODE in the $\mathcal{O}(1)$-problem (54) is

$$\phi_0(t) = -c_3 e^{-\frac{1}{2}t} + (c_3 r - c_4\omega)t e^{-\frac{1}{2}t} + c_3\cos(\omega t) + c_4\sin(\omega t). \tag{77}$$

The solution of the $\mathcal{O}(\varepsilon)$-problem in (76) is

$$\begin{aligned} \phi_1(t) = {} & (\mathcal{A}_1 + \mathcal{B}_1 t)e^{-\frac{t}{2}} + \phi_{1,P}(t) + e^{-\frac{3t}{2}}\sum_{m=0}^{3} U_m t^m + e^{-t}\sum_{m=0}^{2}\left(v_m\cos(\omega t) + \nu_m\sin(\omega t)\right)t^m \\ & + t^2 e^{-\frac{t}{2}}(d_0 + d_1 t) + e^{-\frac{t}{2}}\sum_{m=0}^{1}\left(\hat{v}_m\cos(2\omega t) + \hat{\nu}_m\sin(2\omega t)\right)t^m, \end{aligned} \tag{78}$$

where all extended variables are given in Appendix B.5.

Using the result in (77) and (78), it follows from (52), the approximation ϕ_a for ϕ in (22) is given by

$$\phi_a(t - x) = \phi_0(t - x) + \varepsilon\phi_1(t - x) \tag{79}$$

We can see that the nonlinearity ε affects the change in frequency. Fig. 13 provides a detailed illustration of the incident wave, coming from the right side to the boundary $(x = 0)$, and the reflected wave, shown as distinct lines, with the parameter $k = 1$.

In this case, with a small linear spring constant $p = \frac{1}{4}$ and weak damping $\hat{\beta}$, the boundary approximates a free-end condition, resulting in the reflected wave adopting an even symmetry relative to the incoming wave, as shown in Fig. 13a and c. Consequently, the interaction between the incoming and reflected waves at the boundary produces a higher maximum amplitude, as shown in Fig. 13b.

Fig. 13 illustrates the dependence of the characteristics of the reflected wave on the natural frequency ω, as reflected in the governing Eq. (79), where each term varies with ω. This shift highlights the sensitivity of wave reflection symmetry to changes in natural frequency [27].

4.5.3. Case 3: $p > \frac{1}{4}$ and $\beta = \mathcal{O}(\varepsilon)$

It follows from (36) and (70) that:

$$\begin{cases} \mathcal{A}_0(0) = -c_3, \\ \mathcal{B}_0(0) = \frac{rc_3 - \omega c_4}{\mu} \end{cases} \tag{80}$$

Again, to remove secular terms in ϕ_1, it follows from Appendix B.6 and from (67) that $\mathcal{A}_0(\tau)$ and $\mathcal{B}_0(\tau)$ have to satisfy:

$$\begin{cases} \frac{d\mathcal{A}_0(\tau)}{d\tau} = -\frac{1}{2}\hat{\beta}\mathcal{A}_0(\tau) + \mathcal{K}\mathcal{B}_0(\tau), \\ \frac{d\mathcal{B}_0(\tau)}{d\tau} = -\frac{1}{2}\hat{\beta}\mathcal{B}_0(\tau) - \mathcal{K}\mathcal{A}_0(\tau), \end{cases} \tag{81}$$

with $\mathcal{K} = \frac{\mathcal{H}}{2\mu} - \frac{1}{4\mu}\hat{\beta}$. The solution of (81) is given by:

$$\begin{cases} \mathcal{A}_0(\tau) = e^{-\frac{1}{2}\hat{\beta}\tau}\left[-c_3\cos(\mathcal{K}\tau) + \frac{rc_3 - \omega c_4}{\mu}\sin(\mathcal{K}\tau)\right], \\ \mathcal{B}_0(\tau) = e^{-\frac{1}{2}\hat{\beta}\tau}\left[\frac{rc_3 - \omega c_4}{\mu}\cos(\mathcal{K}\tau) + c_3\sin(\mathcal{K}\tau)\right]. \end{cases} \tag{82}$$

Hence, as an approximation ϕ_a for the unknown function ϕ in (7), we have the following expression:

$$\phi_a(t - x) = -c_3 e^{-\mathcal{J}(t-x)}\cos((\mathcal{K}\varepsilon + \mu)(t - x)) + \frac{rc_3 - \omega c_4}{\mu}e^{-\mathcal{J}(t-x)}\sin((\mathcal{K}\varepsilon + \mu)(t - x)) + c_3\cos(\omega(t - x)) + c_4\sin(\omega(t - x), \tag{83}$$

with $\mathcal{J} = \frac{1}{2}\hat{\beta}\varepsilon + \frac{1}{2}$.

From our solution (83), we can see that the nonlinearity parameter ε influences the amplitude. To illustrate how the wave reflected at the boundary, we present Fig. 14 and take $k = 1$.

Based on Fig. 14a (and the magnified view in Fig. 14b), selecting a low natural frequency $\omega = 1$ reveals significant changes in wave behavior as p increases beyond $p > \frac{1}{4}$. For smaller values of p (e.g., $p = \frac{1}{3}$ or $p = 1$), the reflected waves exhibit even extension behavior observed for various damping values $\hat{\beta}$, given their $\mathcal{O}(\varepsilon)$ order magnitude in this problem. In contrast, as p increases (depicted by the yellow line), the reflection transitions to an odd extension. These findings align with previous cases, highlighting the critical role of the spring coefficient p in determining wave symmetry based on its relative magnitude.

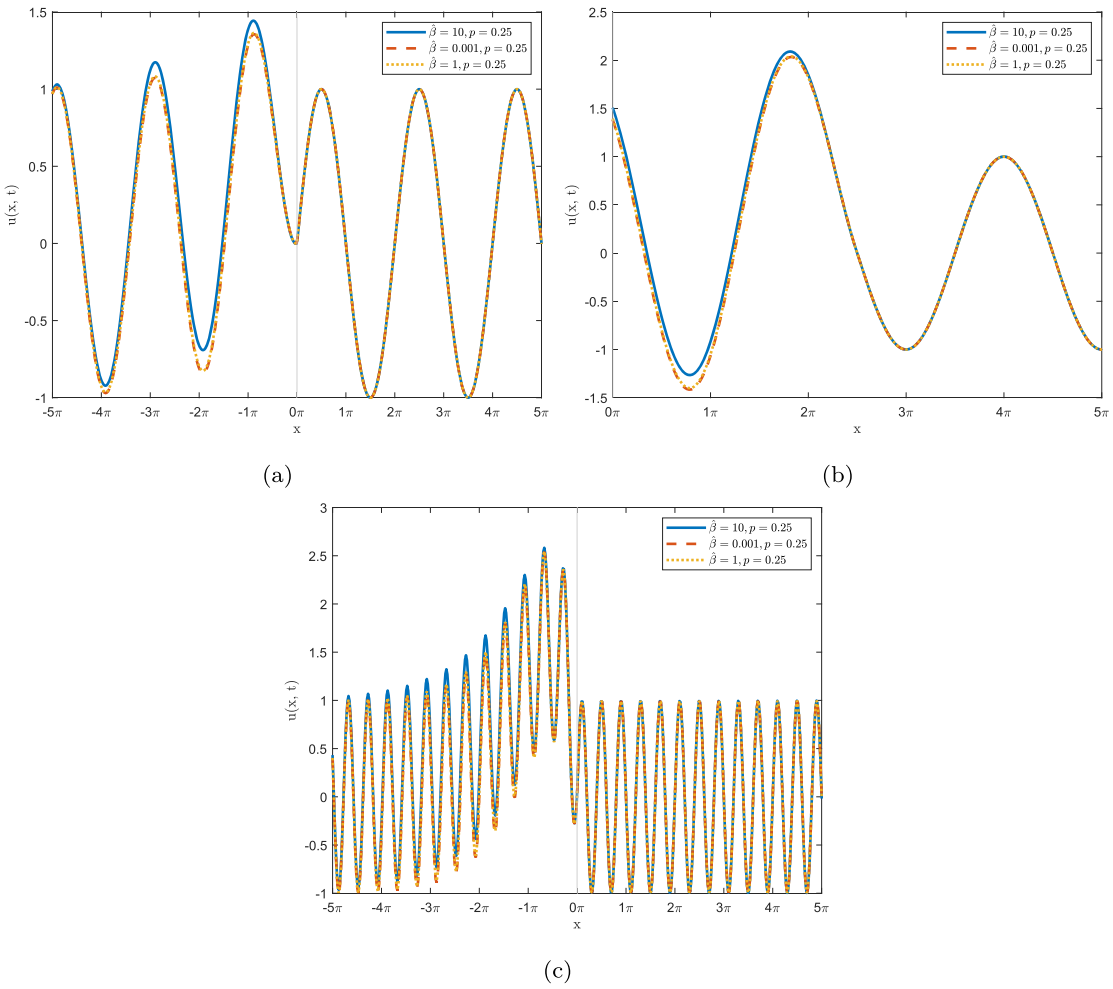

Fig. 13. Continuous sine wave and it's reflection for $\tilde{m} \neq 0$ and $\varepsilon \neq 0$ for case $\hat{\beta} = \mathcal{O}(\epsilon)$, $p = \frac{1}{4}$, and: (a) $\omega = 1$, $\varepsilon = 0.01$, at $t = 0$; (b) $\omega = 1$, $\varepsilon = 0.01$, at $t = \frac{5}{2}\pi$; (c) $\omega = 5$, $\varepsilon = 0.001$, at $t = 0$.

We also illustrate the interaction between the incoming waves and their reflections at the boundary $t = \frac{5\pi}{2}$, as shown in Fig. 14c. As in previous cases, even extension of the reflection amplifies the combined wave amplitude at certain times.

At higher frequencies, the interaction between damping and spring constants remains evident in suppressing the reflected wave's return to its natural incoming wave frequency. Increased spring and damping coefficients accelerate this process, as shown in Fig. 14d.

4.6. Numerical comparisons

In the preceding section, approximate solutions to the nonlinear problem were obtained using the MSP method. To assess their accuracy, the same governing equation is now solved numerically, without relying on small-displacement assumptions. A fourth-order Runge–Kutta (RK4) scheme is used to compute reference solutions for identical parameter values, enabling a direct comparison with the MSP results.

The governing PDE is first discretized in space using a second-order central finite-difference scheme, resulting in a system of ODEs,

$$\begin{cases} y'(t) &= \mathbf{F}(t, y), \qquad t > t_0, \\ y(t_0) &= y_0, \end{cases} \tag{84}$$

where $y(t)$ denotes the vector of discrete solution variables and $\mathbf{F}$ represents the spatially discretized operator, including boundary contributions [41].

Time integration is performed using the classical RK4 method. For a given time step Δt, the solution is advanced from t^n to $t^{n+1} = t^n + \Delta t$ as

$$\mathbf{k}_1 = \mathbf{F}(y^n, t^n),$$

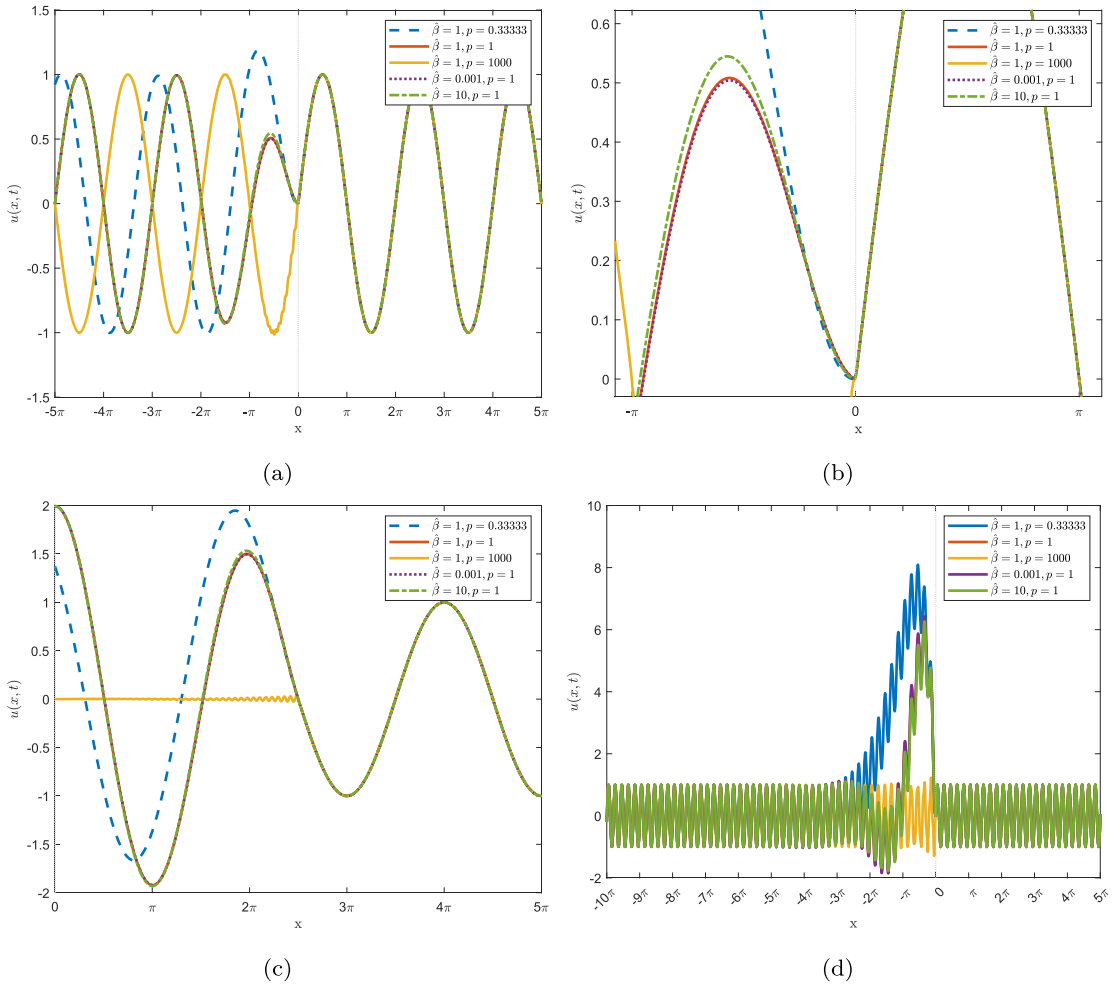

Fig. 14. A continuous sine wave and its reflections at the boundary for the problem $\tilde{m} \neq 0$ and $\varepsilon \neq 0$ for the case $\hat{\beta} = \mathcal{O}(\varepsilon)$, $p > \frac{1}{4}$, and: (a) $\omega = 1$, $\varepsilon = 0.01$, at $t = 0$; (b) $\omega = 1$, $\varepsilon = 0.01$, at $t = 0$ (zoomed); (c) $\omega = 1$, $\varepsilon = 0.01$, at $t = \frac{5}{2}\pi$; (d) $\omega = 10$, $\varepsilon = 0.01$, at $t = 0$.

$$\mathbf{k}_2 = \mathbf{F}\Big(y^n + \tfrac{\Delta t}{2}\mathbf{k}_1,\, t^n + \tfrac{\Delta t}{2}\Big),$$
$$\mathbf{k}_3 = \mathbf{F}\Big(y^n + \tfrac{\Delta t}{2}\mathbf{k}_2,\, t^n + \tfrac{\Delta t}{2}\Big),$$
$$\mathbf{k}_4 = \mathbf{F}\big(y^n + \Delta t\,\mathbf{k}_3,\, t^n + \Delta t\big).$$

Hence, at t^{n+1}, the following solution is approximated by

$$y^{n+1} = y^n + \frac{\Delta t}{6}\big(\mathbf{k}_1 + 2\mathbf{k}_2 + 2\mathbf{k}_3 + \mathbf{k}_4\big). \tag{85}$$

In the following comparisons, we will take $\Delta t = \frac{1}{10}$. When stability holds, the global truncation error is $\mathcal{O}(10^{-4})$. By plotting the numerical solution ϕ_n from the RK4 method and comparing it with the analytical solution ϕ_a, we can study the difference between the two approximations. In these plots, we use the same values as in the previous sections.

4.6.1. Numerical comparison for the problem with $\tilde{m} = 0$ and $\varepsilon \neq 0$

It follows from (6), (7), and (20), the initial-value problem (IVP) is given as follows:

$$\begin{cases} \phi'(t) = -\frac{p}{1+\beta}[\phi(t) + \psi(t)] - \frac{\varepsilon}{1+\beta}[\phi(t) + \psi(t)]^3 + \frac{1-\beta}{1+\beta}\psi(t), \\ \phi(0) = \frac{1}{2}f(0). \end{cases} \tag{86}$$

Taking the ICs (28), we compare ϕ_n and ϕ_a with $\varepsilon = 0.01$. Fig. 15 shows the comparison between the two solutions.

In Fig. 15a, the numerical solution exhibits a behavior that is in close agreement with the analytical solution. To further quantify this agreement, we examine the absolute difference between the two, since both solutions are approximate and may attain zero values.

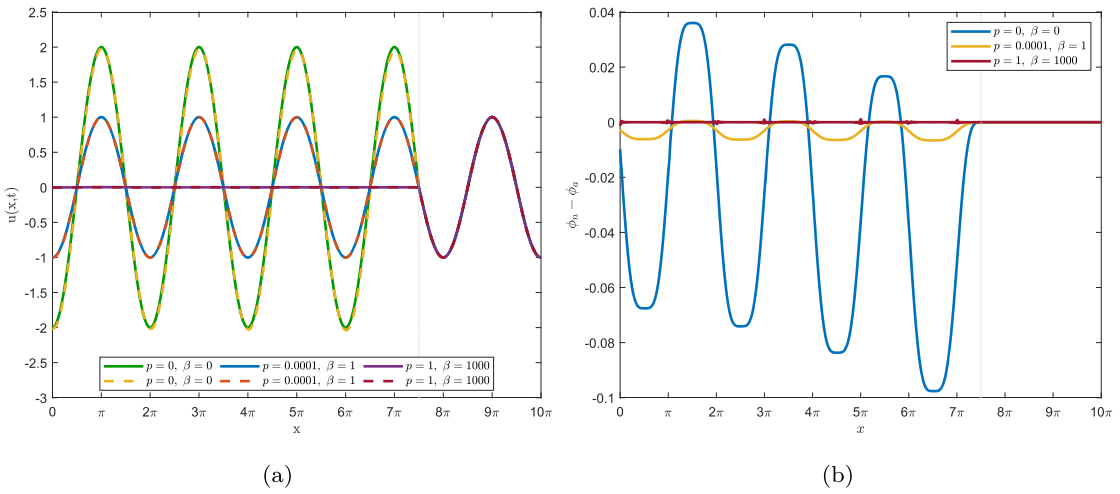

Fig. 15. Comparison and difference between numerical (ϕ_n) and analytical (ϕ_a) solutions for a continuous sine wave and its reflections at the boundary for the parameter values $\tilde{m} = 0$, $\varepsilon \neq 0$, at $t = 7.5\pi$: (a) ϕ_n (dashed lines) vs ϕ_a (solid lines). (b) $\phi_n - \phi_a$.

For all combinations considered of p and β, the differences between the two solutions remain small (< 0.1) (Fig. 15b) compared to the maximum wave amplitude under superposition, which is 2. The analysis within the MSP framework is conducted under the assumption of small displacements. Consequently, the largest discrepancies occur near the free end, where repeated wave arrivals and reflections accumulate numerical errors due to continuous interaction between the incident and reflected waves.

4.6.2. *Numerical comparison on the problem with $\tilde{m} \neq 0$ and $\varepsilon \neq 0$*

In this subsection, we will focus on the $\beta = \mathcal{O}(1)$ problem (4.4). We introduce the auxiliary state variables

$$y_1(t) = \phi(t), \qquad y_2(t) = \phi'(t). \tag{87}$$

From (31), it follows that the first-order system yields

$$\begin{cases} y_1'(t) &= y_2(t), \\ y_2'(t) &= -(1+\beta)\, y_2(t) - p\, y_1(t) - \varepsilon(y_1(t) + \psi(t))^3 - \psi''(t) + (1-\beta)\psi'(t) - p\psi(t). \end{cases} \tag{88}$$

The resulting system (88) is well posed as an IVP upon specification of the ICs

$$\begin{cases} y_1(0) = \phi(0) = \frac{1}{2} f(0), \\ y_2(0) = \phi'(0) = -\frac{1}{2} f'(0) + \frac{1}{2} g(0). \end{cases} \tag{89}$$

In this problem, three damping regimes are investigated, namely the cases with overdamping ($(1+\beta)^2 > 4p$), critically damped ($(1+\beta)^2 = 4p$), and underdamping ($(1+\beta)^2 < 4p$), as identified from the analytical solution.

Fig. 16 presents a comparative visualization of the reflected wave response obtained from the analytical and numerical solutions in all the cases considered. The results are shown for $\varepsilon = 0.01$ at $t = 7.5\pi$. In all cases, the discrepancy between ϕ_n and ϕ_a remains small (< 0.1) compared to the maximum wave amplitude under superposition, which is 2. Larger discrepancies are observed for small values of p and β. In this regime, the boundary behaves as a weakly constrained and weakly dissipative oscillator, allowing reflected waves to persist and repeatedly interact with it. This increases sensitivity to phase errors and amplifies higher-order nonlinear effects that are not captured by the leading-order analytical approximation, as illustrated by the blue curves in Fig. 16b, d, and f. As p and β increase, boundary oscillations decay more rapidly, and the response becomes increasingly dominated by a single mode, leading to closer agreement between the numerical and analytical solutions and a more uniform error distribution. Hence, if, for some time, the amplitudes become larger (or smaller), the errors also become larger (or smaller).

An analogous conclusion applies to the $\beta = \mathcal{O}(\varepsilon)$ in problem (4.5). Here, due to the small damping, the behavior of the reflected wave is primarily governed by the spring stiffness, with distinct responses arising for $p < \frac{1}{4}$, $p = \frac{1}{4}$, and $p > \frac{1}{4}$, consistent with the classification established earlier.

4.7. *The energy and its rate of change*

4.7.1. *The case $m = 0$ and $\varepsilon = 0$*

In this case, the total energy $E(t)$ is the sum of the kinetic and potential energies of the string and the potential energy of the spring, that is

$$E(t) = \frac{1}{2} \int_0^\infty \left(u_t^2(x,t) + u_x^2(x,t)\right) \mathrm{d}x + \frac{1}{2} p u^2(0,t). \tag{90}$$

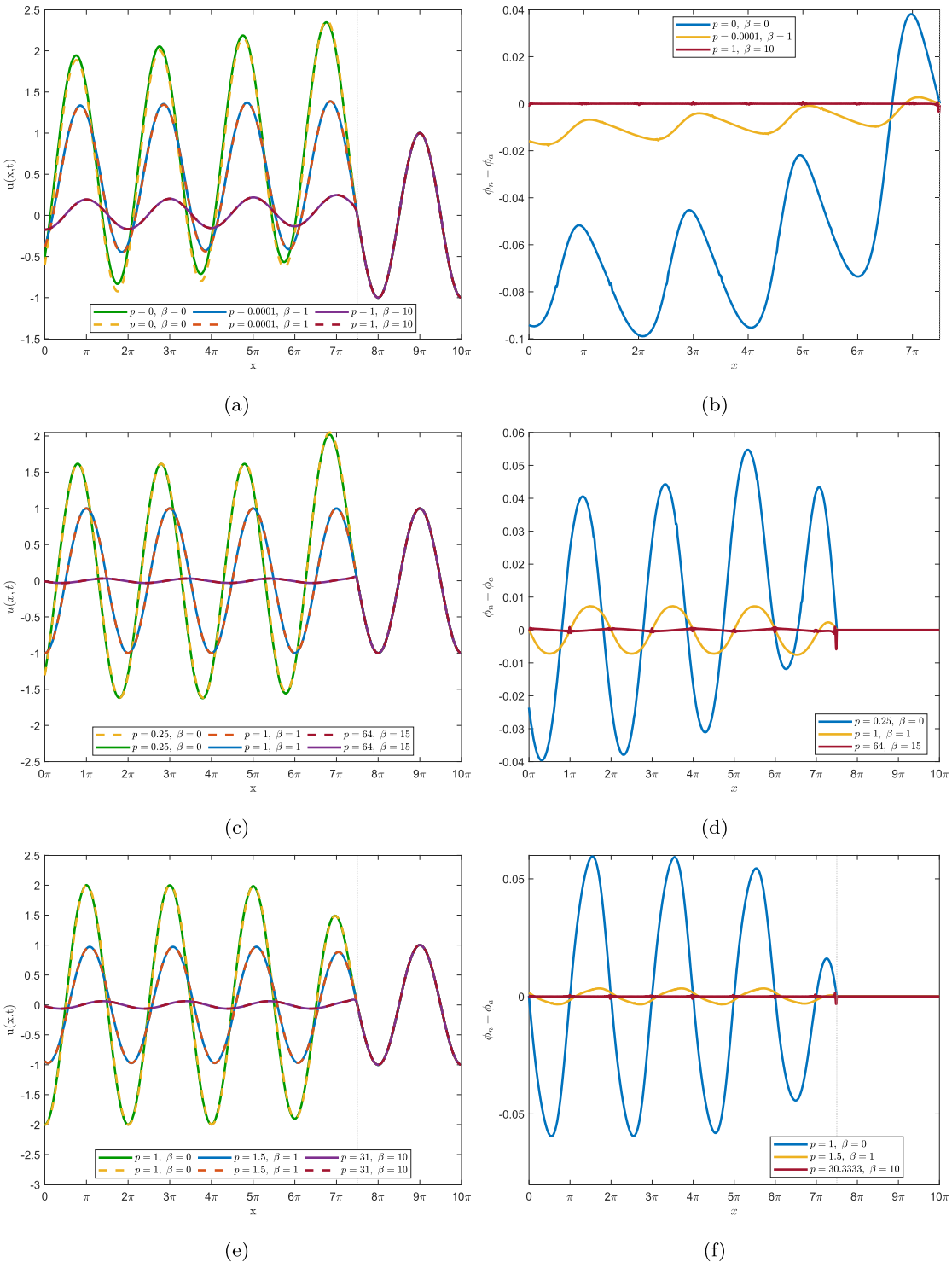

Fig. 16. Comparison and difference between ϕ_n (dashed lines) and ϕ_a (solid lines) for a continuous sine wave and its reflections at the boundary for the parameter values $\tilde{m} = 0$, $\varepsilon \neq 0$, and $\beta = \mathcal{O}(1)$ at $t = 10\pi$. For $(1+\beta)^2 > 4p$: (a) ϕ_n vs ϕ_a, (b) $\phi_n - \phi_a$. For $(1+\beta)^2 = 4p$: (c) ϕ_n vs ϕ_a, (d) $\phi_n - \phi_a$. For $(1+\beta)^2 < 4p$: (e) ϕ_n vs ϕ_a, (f) $\phi_n - \phi_a$.

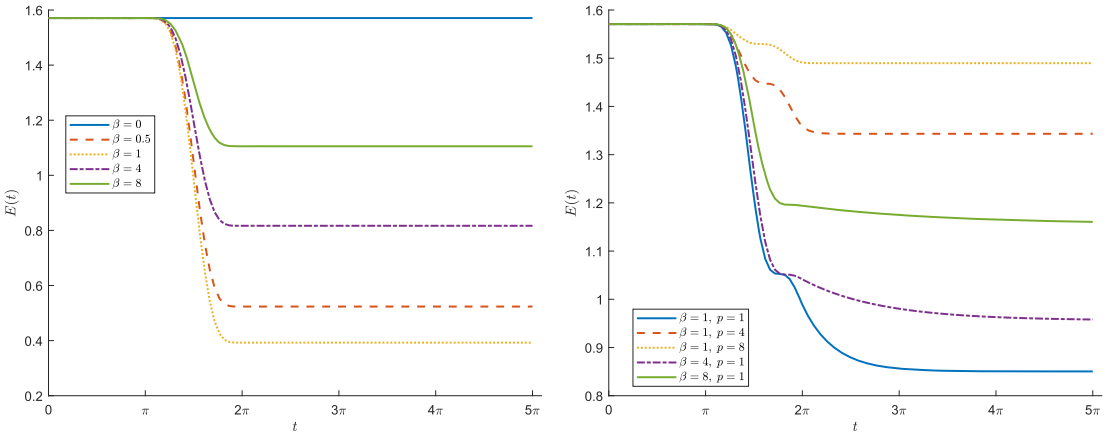

Fig. 17. The energy dissipation for the Problem $m = 0$ and $\varepsilon = 0$. (a) $p = 0$. (b) $\beta \neq 0$; $p \neq 0$.

Taking the time derivative of $E(t)$, we find

$$\begin{aligned}\frac{\mathrm{d}E(t)}{\mathrm{d}t} &= \int_0^\infty \left[u_t u_{tt} + u_x u_{xt}\right]\mathrm{d}x + pu(0,t)u_t(0,t),\\ &= \int_0^\infty u_t u_{tt}\,\mathrm{d}x + \int_0^\infty u_x u_{xt}\,\mathrm{d}x + pu(0,t)u_t(0,t),\\ &= \int_0^\infty u_t u_{tt}\,\mathrm{d}x + \int_0^\infty u_x \frac{\mathrm{d}u_t}{\mathrm{d}x}\,\mathrm{d}x + pu(0,t)u_t(0,t),\\ &= \int_0^\infty u_t u_{tt}\,\mathrm{d}x + \left[u_x u_t\right]_0^\infty - \int_0^\infty u_{xx}u_t\,\mathrm{d}x + pu(0,t)u_t(0,t)\\ &= \int_0^\infty u_t\left(u_{tt} - u_{xx}\right)\mathrm{d}x + \left[u_x u_t\right]_0^\infty + pu(0,t)u_t(0,t).\end{aligned} \tag{91}$$

We know from Eq. (2) that $u_{tt} - u_{xx} = 0$, therefore

$$\frac{\mathrm{d}E(t)}{\mathrm{d}t} = \left[u_x u_t\right]_0^\infty + pu(0,t)u_t(0,t). \tag{92}$$

Observing that there is no energy at $x = \infty$, we deduce that

$$\frac{\mathrm{d}E(t)}{\mathrm{d}t} = -u_x(0,t)u_t(0,t) + pu(0,t)u_t(0,t). \tag{93}$$

Given our BC (2), that is, $u_x(0,t) = pu(0,t) + \beta u_t(0,t)$, we obtain

$$\begin{aligned}\frac{\mathrm{d}E(t)}{\mathrm{d}t} &= -\left(pu(0,t) + \beta u_t(0,t)\right)u_t(0,t) + pu(0,t)u_t(0,t),\\ &= -\beta u_t^2(0,t).\end{aligned} \tag{94}$$

Then,

$$\frac{\mathrm{d}E(t)}{\mathrm{d}t} = -\beta u_t^2(0,t) \leq 0. \tag{95}$$

This implies that the energy $E(t)$ decreases over time.

Fig. 17 illustrates the energy dissipation for the spring-damper case for the ICs $u(x,0) = f(x), u_t(x,0) = g(x)$ with

$$f(x) = \begin{cases}\sin^2(x), & \text{for } 2\pi \leq x \leq 3\pi,\\ 0, & \text{elsewhere.}\end{cases}; \quad g(x) = \begin{cases}\sin(2x), & \text{for } 2\pi \leq x \leq 3\pi,\\ 0, & \text{elsewhere.}\end{cases} \tag{96}$$

In Fig. 17a, the spring coefficient is set to $p = 0$. The illustration shows that the system's energy remains conserved when $\beta = 0$, consistent with Eq. (95), where $E(t) = E(0)$ holds for $\beta = 0$. We also see that under the ideal damping configuration (as described in Section 1), energy dissipates at the fastest rate compared to other scenarios, as illustrated by the yellow line in Fig. 17a. However, as the damping coefficient β increases, the dashpot's movement becomes increasingly constrained, leading to a slower rate of energy dissipation over time. This result confirms the work in [22]. These findings also align with the results in [33], where the energetics of a semi-infinite traveling string with nonclassical boundary support are analyzed.

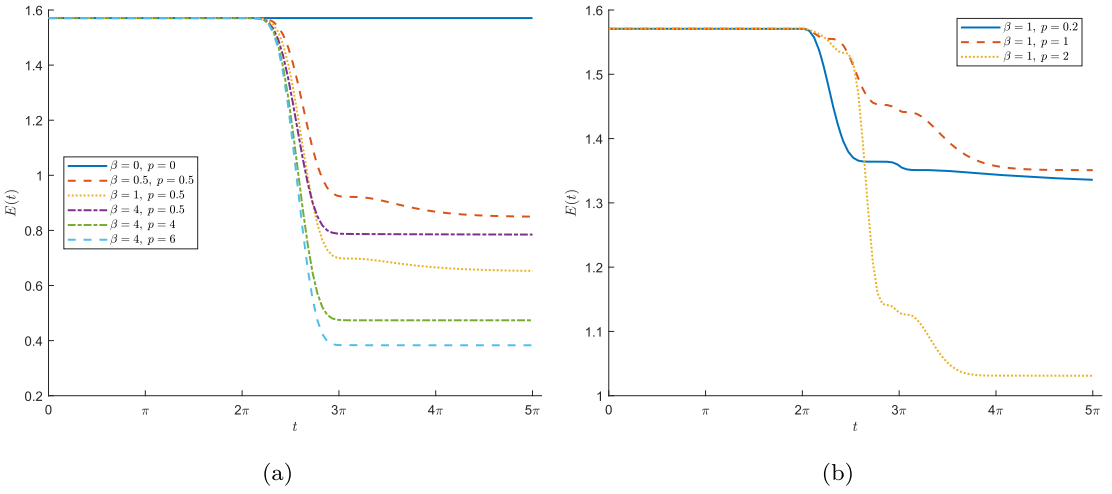

Fig. 18. The energy dissipation for the Problem $m \neq 0$ and $\varepsilon = 0$. (a) varying β and p for case 1. (b) $\beta = 1$, varying p in E(t).

Additionally, Fig. 17b shows that, for a fixed β, increasing the spring coefficient p results in a comparatively lower rate of energy dissipation than when β is allowed to vary with p kept constant. This indicates a nuanced dependence of the energy dissipation on the relative magnitudes of β and p, suggesting that the energy dynamics of the system are more sensitive to changes in the damping coefficient than in the spring coefficient.

4.7.2. The case $m \neq 0$ and $\varepsilon = 0$

In this case, the total energy $E(t)$ is the sum of the kinetic and potential energies of the string and the potential energy of the spring, and the kinetic energy of the mass m, that is,

$$E(t) = \frac{1}{2}\int_0^\infty \left(u_t^2(x,t) + u_x^2(x,t)\right)\mathrm{d}x + \frac{1}{2}u_t^2(0,t) + \frac{1}{2}pu^2(0,t). \tag{97}$$

Just like in Section 4.7.1, we take the time derivative of $E(t)$, and considering PDE in (2), we will have:

$$\frac{\mathrm{d}E(t)}{\mathrm{d}t} = \left[u_x u_t\right]_0^\infty + u_t(0,t)u_{tt}(0,t) + pu(0,t)u_t(0,t). \tag{98}$$

Observing that there is no energy at $x = \infty$, and given our BC $u_x(0,t) = u_{tt}(0,t) + pu(0,t) + \beta u_t(0,t)$, we have

$$\frac{\mathrm{d}E(t)}{\mathrm{d}t} = -\beta u_t^2(0,t) \leq 0. \tag{99}$$

Hence, the energy is bounded if the initial energy is bounded.

Fig. 18 illustrates the energy dissipation given the ICs (96). The figure illustrates the energy decay over time t caused by the mass-spring-dashpot system. The energy remains conserved when the damping coefficient $\beta = 0$. In the over-damped scenario, as shown in Fig. 18a, the interplay between the damping β and the spring coefficient p significantly influences the energy dissipation. When the spring coefficient is fixed at $p = 0.5$, most energy dissipation occurs at $\beta = 1$, a result consistent with the findings from the previous subsection. Conversely, when β is fixed, increasing the spring coefficient leads to faster energy dissipation. This is evident in Fig. 18a for $\beta = 4$ and in Fig. 18b for $\beta = 1$.

4.7.3. In the case $m = 0$ and $\varepsilon \neq 0$

In this case, the total energy $E(t)$, compared to Section 4.7.1, includes a nonlinear term due to the nonlinearity of the spring, and is given by:

$$E(t) = \frac{1}{2}\int_0^\infty \left(u_t^2(x,t) + u_x^2(x,t)\right)\mathrm{d}x + \frac{1}{2}pu^2(0,t) + \frac{\varepsilon}{4}u^4(0,t). \tag{100}$$

Since we know from eq. (2) that $u_{tt} - u_{xx} = 0$, and by taking the time derivative of $E(t)$, we find

$$\frac{\mathrm{d}E(t)}{\mathrm{d}t} = \left[u_x u_t\right]_0^\infty + pu(0,t)u_t(0,t) + \varepsilon u^3(0,t)u_t(0,t). \tag{101}$$

Observing that there is no energy at $x = \infty$, and given our BC $u_x(0,t) = pu(0,t) + \beta u_t(0,t) + \varepsilon u^3(0,t)$, we have

$$\frac{\mathrm{d}E(t)}{\mathrm{d}t} = -\beta u_t^2(0,t) \leq 0. \tag{102}$$

This implies that the energy $E(t)$ decreases over time. We illustrate in Fig. 19 the energy dissipation for the ICs given in (96).

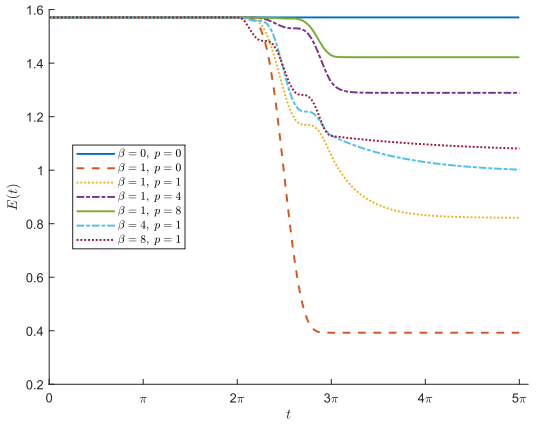

Fig. 19. The energy dissipation for the Problem $m = 0$ and $\varepsilon \neq 0$.

The illustration confirms that the system's energy is conserved when $\beta = 0$, consistent with Eq. (102), where $E(t) = E(0)$. In the ideal damping configuration (Section 1), the energy dissipates most rapidly, as shown by the red dotted line in Fig. 19. However, as β increases, the damper's motion becomes restricted, slowing energy dissipation. In addition, it is evident that for a fixed β, increasing the spring coefficient p results in a slower rate of energy dissipation than varying β while keeping p constant. This highlights the energy dissipation dynamics of the system, which is more sensitive to changes in the damping coefficient than to changes in the spring coefficient.

4.7.4. *The case $m \neq 0$ and $\varepsilon \neq 0$*

In this case, the total energy $E(t)$ of the string and the mass-spring-damper system with a cubic nonlinear spring property is given by

$$E(t) = \frac{1}{2}\int_0^\infty \left(u_t^2(x,t) + u_x^2(x,t)\right)\mathrm{d}x + \frac{1}{2}u_t^2(0,t) + \frac{1}{2}pu^2(0,t) + \frac{\varepsilon}{4}u^4(0,t). \tag{103}$$

Taking the time derivative of $E(t)$, we can again deduce that

$$\frac{\mathrm{d}E(t)}{\mathrm{d}t} = -\beta u_t^2(0,t) \leq 0, \tag{104}$$

and so,

$$E(t) \leq E(0), \quad \text{for all } t \geq 0. \tag{105}$$

Fig. 20 depicts the total energy decay over time t in the mass-spring-dashpot system and in the string, with the nonlinear spring coefficient $\varepsilon = 0.01$, $\omega = 1$, $k = 1$, and the ICs given in (96). From the figure, we see that the energy remains conserved when the damping coefficient is $\beta = 0$. When the damping coefficient $\beta > 0$, it is evident from Eq. (104) and Fig. 20 that the system's energy is dissipated. The interaction between β and the spring coefficient p plays a crucial role in energy dissipation. With p fixed at 0.5, higher values of β result in faster energy dissipation (see red and yellow lines). Similarly, when β is fixed (in this case, $\beta = 1$), increasing p from $p = 1$ (purple line) to $p = 1.5$ (green line) accelerates energy dissipation. Previous studies have also indicated that energy is influenced by coefficients determined by BCs [13,42].

5. Conclusion

In this paper, the behavior of reflected waves in semi-infinite strings under various linear and cubic nonlinear BCs was analyzed analytically using D'Alembert's method and numerically using the RK4 Method and a central finite difference scheme. Four types of tuned-mass-damper systems were considered at the boundary: (1) a damper-linear spring system, (2) a mass-damper-linear spring system, (3) a damper-nonlinear spring system, and (4) a mass-damper-nonlinear spring system.

Across the scenarios, the BC strongly determines the nature of wave reflection. A fixed end produces an odd reflection of the incoming wave such that the superposition of the incoming and reflected waves enforces zero displacement at the boundary. A free end generates an even reflection, resulting in-phase superposition and amplitude doubling. Under ideal damping, the incoming wave is fully absorbed at the boundary, suppressing reflection, and eliminating wave amplification. Furthermore, the mass-spring-damper system distorts the reflected waves, causing the reflected wave length to elongate.

For the nonlinear BC, the solution is approximated using the MSP method. The analysis shows that boundary nonlinearity plays a crucial role in determining the behavior of the reflected wave. In particular, the nonlinear boundary produces an elongated reflected wave compared to the response due to a linear BC.

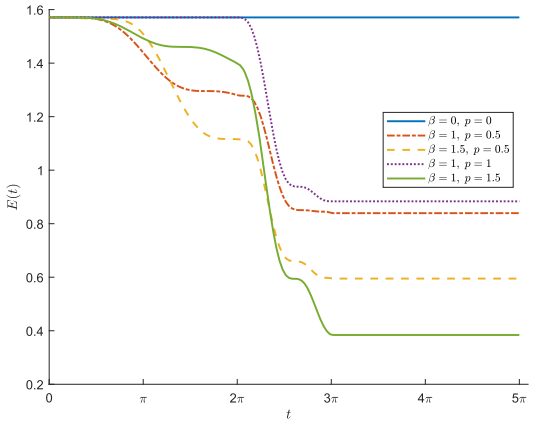

Fig. 20. The energy dissipation for the Problem $m \neq 0$ and $\varepsilon \neq 0$.

In problem four, we consider two different time scales ($\mathcal{O}(1)$ and $\mathcal{O}(\varepsilon)$) for the damping coefficient β. This variation leads to different behavioral conditions. For β being $\mathcal{O}(1)$, the behavior depends on the relative values of β and p. On the other hand, when we have weak damping (as β is $\mathcal{O}(\varepsilon)$), the value of p was the only factor for which the system leads to over-damping, critically damping, or under-damping. Specifically, when β is $\mathcal{O}(\varepsilon)$, reflected waves in the over-damped and in the critically damped cases generally exhibit even extensions due to system constraints. In contrast, odd extensions occur in underdamped conditions due to high spring constants. For all cases in Problem 4, we conclude that the nonlinearity significantly influences the vibrations. Furthermore, the nonlinear problem is solved numerically using an RK4 scheme. The numerical response closely follows the MSP approximation, indicating that both methods capture the same underlying dynamics, with only minor discrepancies in amplitude.

Lastly, we analyzed the energy dissipation for both spring-damper and mass-spring-damper cases. In all cases, the energy is conserved when the damping parameter $\beta = 0$. In the spring-damper case, the energy dissipation dynamics are more sensitive to changes in the damping parameter than to changes in the spring coefficient. Moreover, when the damping coefficient $\beta = 1$, the energy dissipates optimally at the boundary. However, as the damping coefficient increases, the damper's movement becomes more constrained, leading to lower energy dissipation over time. For the spring-mass-damper system, we can see that when $\beta = 1$, increasing the spring coefficient leads to a higher energy dissipation.

Future research will focus on analyzing the impact of nonlinearities in the damping coefficient to better understand its influence on wave dynamics. Additionally, this methodology can be extended to investigate other types of nonlinearities, providing a versatile framework for exploring complex system behavior in similar settings.

CRediT authorship contribution statement

Jeri Araiku: Formal analysis, Methodology, Software, Visualization, Writing – original draft, Writing – review & editing; **Wim T. van Horssen:** Conceptualization, Supervision, Validation.

Data availability

Data will be made available on request.

Declaration of competing interest

The authors declare that there is no conflict of interest with respect to the publication of this article.

The authors declare that they have no known competing financial interests or personal relationships that could have appeared to influence the work reported in this paper.

Acknowledgments

This article is part of a PhD research project. The authors wish to express their profound gratitude to Indonesia's Ministry of Finance for funding this research through the Indonesia Endowment Fund for Education Agency (LPDP) scholarship grant number SKPB-1953/LPDP/LPDP.3/2023. Additionally, we extend our heartfelt thanks to Delft University of Technology for providing outstanding facilities that ensured the efficient conduct of this research. We also thank the anonymous reviewers for their valuable comments, which helped improve our paper.

Appendix A. Parameter definition in Section 4.2 Case $(1+\beta)^2 < 4p$.

$$F_c(\hat{t}) = \int_0^{\hat{t}} \mathrm{e}^{\theta s}\cos(\kappa s)\, f(s)\,\mathrm{d}s.$$
$$F_s(\hat{t}) = \int_0^{\hat{t}} \mathrm{e}^{\theta s}\sin(\kappa s)\, f(s)\,\mathrm{d}s.$$
$$G_c(\hat{t}) = \int_0^{\hat{t}} \mathrm{e}^{\theta s}\cos(\kappa s)\, g(s)\,\mathrm{d}s.$$
$$G_s(\hat{t}) = \int_0^{\hat{t}} \mathrm{e}^{\theta s}\sin(\kappa s)\, g(s)\,\mathrm{d}s.$$
$$H_c(\hat{t}) = \int_0^{\hat{t}} \mathrm{e}^{\theta s}\cos(\kappa s)\Big(\int_0^{s} g(v)\,dv\Big)\,\mathrm{d}s.$$
$$H_s(\hat{t}) = \int_0^{\hat{t}} \mathrm{e}^{\theta s}\sin(\kappa s)\Big(\int_0^{s} g(v)\,dv\Big)\,\mathrm{d}s.$$

Appendix B. Secular terms

B.1. $\beta = \mathcal{O}(1)$, case 1

To ensure that our solution stays bounded, we need to eliminate the secular terms. First, we should find all secular terms in $\psi^3(t)$, $\phi_{0_{t\tau}}$, ϕ_{0_τ}, ϕ_0^3, $\phi_0^2\,\psi(t)$ and $\phi_0\psi^2(t)$ as follows:

$$\begin{aligned}
\psi^3(t):&\quad \text{does not contain secular terms.}\\
\phi_{0_{t\tau}}:&\quad \frac{\mathrm{d}\mathcal{A}_0(\tau)}{\mathrm{d}\tau}r_1\mathrm{e}^{r_1 t}+\frac{\mathrm{d}\mathcal{B}_0(\tau)}{\mathrm{d}\tau}r_2\mathrm{e}^{r_2 t}.\\
\phi_{0_\tau}:&\quad \frac{\mathrm{d}\mathcal{A}_0(\tau)}{\mathrm{d}\tau}\mathrm{e}^{r_1 t}+\frac{\mathrm{d}\mathcal{B}_0(\tau)}{\mathrm{d}\tau}\mathrm{e}^{r_2 t}.\\
\phi_0^3:&\quad -\tfrac{3}{2}(c_1^2+c_2^2)\big(\mathcal{A}_0(\tau)\mathrm{e}^{r_1 t}+\mathcal{B}_0(\tau)\mathrm{e}^{r_2 t}\big).\\
\phi_0^2\psi(t):&\quad -kc_2\big(\mathcal{A}_0(\tau)\mathrm{e}^{r_1 t}+\mathcal{B}_0(\tau)\mathrm{e}^{r_2 t}\big).\\
\phi_0\psi^2(t):&\quad \tfrac{1}{2}k^2\big(\mathcal{A}_0(\tau)\mathrm{e}^{r_1 t}+\mathcal{B}_0(\tau)\mathrm{e}^{r_2 t}\big).
\end{aligned}$$

B.2. $\beta = \mathcal{O}(1)$, case 2

The full extension of all variables of the solution of Problem $m \neq 0, \varepsilon \neq 0$, and $(1+\beta)^2 = 4p$ are given as follows

$$\begin{aligned}
\mathcal{A}_1 &= -(a_1+a_3+U_0+v_0+\hat{v}_0),\\
\mathcal{B}_1 &= -r(a_1+a_3+U_0+v_0+\hat{v}_0)-\Big[\omega(b_1+3b_3)+(3rU_0+U_1)+(2rv_0+v_1+\omega v_0)+(\hat{v}_1+2\omega\hat{v}_0+r\hat{v}_0)\Big],\\
\phi_{1,P}(t) &= a_1\cos(\omega t)+b_1\sin(\omega t)+a_3\cos(3\omega t)+b_3\sin(3\omega t),\\
K_1 &= -\tfrac{3}{4}c_1(c_1^2+c_2^2)-\tfrac{3}{2}kc_1c_2-\tfrac{3}{4}k^2c_1,\\
K_2 &= -\tfrac{3}{4}c_2(3c_1^2+c_2^2)-\tfrac{3}{4}kc_1^2-\tfrac{9}{4}k^2c_2-\tfrac{3}{4}k^3,\\
K_5 &= -\tfrac{1}{4}c_1(c_1-3c_2^2)+\tfrac{3}{2}kc_1c_2+\tfrac{3}{4}k^2c_1,\\
K_6 &= -\tfrac{1}{4}c_2(3c_1^2-c_2^2)-\tfrac{3}{4}k(c_1^2-c_2^2)+\tfrac{3}{4}k^2c_2+\tfrac{1}{4}k^3,\\
a_n &= \frac{(p-(n\omega)^2)K_{2n-1}+(1+\beta)n\omega K_{2n}}{(p-(n\omega)^2)^2+((1+\beta)n\omega)^2},\\
b_n &= \frac{(p-(n\omega)^2)K_{2n}-(1+\beta)n\omega K_{2n-1}}{(p-(n\omega)^2)^2+((1+\beta)n\omega)^2},\\
U_3 &= -\frac{\mathcal{B}_0^3}{4r^2},\\
U_2 &= \frac{3}{4r^2}\mathcal{B}_0^2\Big(-\mathcal{A}_0+\frac{\mathcal{B}_0}{r}\Big),\\
U_1 &= \frac{-6r^2\mathcal{A}_0^2\mathcal{B}_0+12r\mathcal{A}_0\mathcal{B}_0^2-9\mathcal{B}_0^3}{8r^2},
\end{aligned}$$

$$
\begin{aligned}
U_0 &= \frac{-2r^3\mathcal{A}_0^3 + 6r^4\mathcal{A}_0^2\mathcal{B}_0 + (3-12r^2)r\mathcal{A}_0\mathcal{B}_0^2 + (9r^2-3)\mathcal{B}_0^3}{8r^5},\\
\upsilon_2 &= -\frac{3\mathcal{B}_0^2}{(r^2+\omega^2)^2}\Big[(r^2-\omega^2)c_1 + 2r\omega(c_2+k)\Big],\\
\nu_2 &= -\frac{3\mathcal{B}_0^2}{(r^2+\omega^2)^2}\Big[(r^2-\omega^2)(c_2+k) - 2r\omega c_1\Big],\\
\upsilon_1 &= \frac{(r^2-\omega^2)X_1 + 2r\omega Y_1}{(r^2+\omega^2)^2},\\
\nu_1 &= \frac{-2r\omega X_1 + (r^2-\omega^2)Y_1}{(r^2+\omega^2)^2},\\
X_1 &= -6\mathcal{A}_0\mathcal{B}_0c_1 - 2S_1,\\
Y_1 &= -6\mathcal{A}_0\mathcal{B}_0(c_2+k) - 2S_2,\\
S_1 &= 2r\upsilon_2 - 2\omega\nu_2,\\
S_2 &= 2\omega\upsilon_2 + 2r\nu_2,\\
\upsilon_0 &= \frac{(r^2-\omega^2)X_0 + 2r\omega Y_0}{(r^2+\omega^2)^2},\\
\nu_0 &= \frac{-2r\omega X_0 + (r^2-\omega^2)Y_0}{(r^2+\omega^2)^2},\\
X_0 &= -3\mathcal{A}_0^2c_1 - (2r\upsilon_1 - 2\omega\nu_1) - 2\upsilon_2,\\
Y_0 &= -3\mathcal{A}_0^2(c_2+k) - (2\omega\upsilon_1 + 2r\nu_1) - 2\nu_2,\\
\tilde{\upsilon}_1 &= \frac{3\mathcal{B}_0}{4\omega^2}T_c,\\
\tilde{\nu}_1 &= \frac{3\mathcal{B}_0}{4\omega^2}T_s,\\
\tilde{\upsilon}_0 &= \frac{3}{4\omega^2}\Big(\mathcal{A}_0T_c - \tfrac{\mathcal{B}_0}{\omega}T_s\Big),\\
\tilde{\nu}_0 &= \frac{3}{4\omega^2}\Big(\mathcal{A}_0T_s - \tfrac{\mathcal{B}_0}{\omega}T_c\Big),\\
T_c &= \tfrac{1}{2}(c_1^2 - c_2^2) - kc_2 - \tfrac{1}{2}k^2,\\
T_s &= c_1c_2 + kc_1.
\end{aligned}
$$

B.3. $\beta = \mathcal{O}(1)$, case 3

All secular terms in $\psi^3(t)$, $\phi_{0_{t\tau}}$, ϕ_{0_τ}, ϕ_0^3, $\phi_0^2\,\psi(t)$ and $\phi_0\psi^2(t)$ as follows:

$$
\begin{aligned}
\psi^3(t) &: \quad \text{does not contain secular terms.}\\
\phi_{0_\tau} &: \quad \frac{\mathrm{d}\mathcal{A}_0(\tau)}{\mathrm{d}\tau}\mathrm{e}^{rt}\cos(\mu t) + \frac{\mathrm{d}\mathcal{B}_0(\tau)}{\mathrm{d}\tau}\mathrm{e}^{rt}\sin(\mu t).\\
\phi_{0_t\tau} &: \quad \left[\frac{\mathrm{d}\mathcal{A}_0(\tau)}{\mathrm{d}\tau}r + \frac{\mathrm{d}\mathcal{B}_0(\tau)}{\mathrm{d}\tau}\mu\right]\mathrm{e}^{rt}\cos(\mu t) + \left[\frac{\mathrm{d}\mathcal{B}_0(\tau)}{\mathrm{d}\tau}r - \frac{\mathrm{d}\mathcal{A}_0(\tau)}{\mathrm{d}\tau}\mu\right]\mathrm{e}^{rt}\sin(\mu t).\\
\phi_0^3 &: \quad \frac{3}{2}\big(c_1^2+c_2^2\big)\big(\mathcal{A}_0(\tau)\mathrm{e}^{rt}\cos(\mu t) + \mathcal{B}_0(\tau)\mathrm{e}^{rt}\sin(\mu t)\big).\\
\phi_0^2\psi(t) &: \quad kc_2\big(\mathcal{A}_0(\tau)\mathrm{e}^{rt}\cos(\mu t) + \mathcal{B}_0(\tau)\mathrm{e}^{rt}\sin(\mu t)\big).\\
\phi_0\psi^2(t) &: \quad \frac{1}{2}k^2\big(\mathcal{A}_0(\tau)\mathrm{e}^{rt}\cos(\mu t) + \mathcal{B}_0(\tau)\mathrm{e}^{rt}\sin(\mu t)\big).
\end{aligned}
$$

B.4. $\beta = \mathcal{O}(\varepsilon)$, case 1

All secular terms in $\psi_t(t)$, $\psi^3(t)$, $\phi_{0_{t\tau}}$, ϕ_{0_t}, ϕ_{0_τ}, ϕ_0^3, $\phi_0^2\,\psi(t)$ and $\phi_0\psi^2(t)$ are given follows:

$$
\begin{aligned}
\psi_t(t) &: \quad \text{does not contain secular terms.}\\
\psi^3(t) &: \quad \text{does not contain secular terms.}\\
\phi_{0_{t\tau}} &: \quad \frac{\mathrm{d}\mathcal{A}_0(\tau)}{\mathrm{d}\tau}r_1\mathrm{e}^{r_1t} + \frac{\mathrm{d}\mathcal{B}_0(\tau)}{\mathrm{d}\tau}r_2\mathrm{e}^{r_2t}.\\
\phi_{0_t} &: \quad r_1\mathcal{A}_0(\tau)\mathrm{e}^{r_1t} + r_2\mathcal{B}_0(\tau)\mathrm{e}^{r_2t}.
\end{aligned}
$$

$$
\begin{aligned}
\phi_{0_\tau}: &\quad \frac{\mathrm{d}\mathcal{A}_0(\tau)}{\mathrm{d}\tau}\mathrm{e}^{r_1 t} + \frac{\mathrm{d}\mathcal{B}_0(\tau)}{\mathrm{d}\tau}\mathrm{e}^{r_2 t}.\\
\phi_0^3: &\quad \frac{3}{2}\left(c_3^2 + c_4^2\right)\left(\mathcal{A}_0(\tau)\mathrm{e}^{r_1 t} + \mathcal{B}_0(\tau)\mathrm{e}^{r_2 t}\right).\\
\phi_0^2\psi(t): &\quad kc_4\left(\mathcal{A}_0(\tau)\mathrm{e}^{r_1 t} + \mathcal{B}_0(\tau)\mathrm{e}^{r_2 t}\right).\\
\phi_0\psi^2(t): &\quad \frac{1}{2}k^2\left(\mathcal{A}_0(\tau)\mathrm{e}^{r_1 t} + \mathcal{B}_0(\tau)\mathrm{e}^{r_2 t}\right).
\end{aligned}
$$

B.5. β in $\mathcal{O}(\varepsilon)$, case 2

The full extension of all variables of the solution of Problem $m \neq 0, \varepsilon \neq 0$, and $p = \frac{1}{4}$ are given as follows

$$
\begin{aligned}
A_1 &= -(a_1 + a_3 + U_0 + \upsilon_0 + \hat{\upsilon}_0),\\
B_1 &= \tfrac{1}{2}(a_1 + a_3) + 2U_0 - U_1 + \tfrac{3}{2}\upsilon_0 - \upsilon_1 - \omega\nu_0 - \omega(b_1 + 3b_3) - d_0 - \hat{\upsilon}_1 - 2\omega\hat{\nu}_0,\\
\phi_{1,P} &= a_1\cos(\omega t) + b_1\sin(\omega t) + a_3\cos(3\omega t) + b_3\sin(3\omega t),\\
Q_n &= \left(\tfrac{1}{4} - (n\omega)^2\right)^2 + (n\omega)^2,\\
a_n &= \frac{\left(\frac{1}{4} - (n\omega)^2\right)K_{2n-1} + (n\omega)K_{2n}}{Q_n},\\
b_n &= \frac{\left(\frac{1}{4} - (n\omega)^2\right)K_{2n} - (n\omega)K_{2n-1}}{Q_n},\\
K_1 &= -\tfrac{3}{4}c_3(c_3^2 + c_4^2) - \tfrac{3}{2}kc_3c_4 - \tfrac{3}{4}k^2c_3 - \hat{\beta}c_4\omega - \hat{\beta}k\omega,\\
K_2 &= -\tfrac{3}{4}c_4(3c_3^2 + c_4^2) - \tfrac{3}{4}kc_3^2 - \tfrac{9}{4}k^2c_4 - \tfrac{3}{4}k^3 + \hat{\beta}\omega c_3,\\
K_5 &= -\tfrac{1}{4}c_3(c_3^2 - 3c_4^2) + \tfrac{3}{2}kc_3c_4 + \tfrac{3}{4}k^2c_3,\\
K_6 &= -\tfrac{1}{4}c_4(3c_3^2 - c_4^2) - \tfrac{3}{4}k(c_3^2 - c_4^2) + \tfrac{3}{4}k^2c_4 + \tfrac{1}{4}k^3,\\
U_3 &= \eta^3,\\
U_2 &= 3c_3\eta^2 + 6\eta^3,\\
U_1 &= 3c_3^2\eta + 12c_3\eta^2 + 18\eta^3,\\
U_0 &= c_3^3 + 6c_3^2\eta + 18c_3\eta^2 + 24\eta^3,\\
\eta &= \tfrac{1}{2}c_3 + c_4\omega,\\
\upsilon_2 &= -\frac{3\eta^2}{\Delta}(m_0c_3 - \omega s),\\
\nu_2 &= -\frac{3\eta^2}{\Delta}(\omega c_3 + m_0\, s),\\
\upsilon_1 &= \frac{6\eta}{\Delta^2}\left[-\Delta m_0c_3^2 + \Delta\omega c_3\, s - \eta m_0^2c_3 - 4\eta\omega^2c_3 - 2\eta m_0^2\, s + 2\eta m_0\omega s + 2\eta\omega^3\, s\right],\\
\nu_1 &= \frac{6\eta}{\Delta^2}\left[-\Delta\omega c_3^2 - \Delta m_0c_3\, s + 2\eta m_0\omega c_3 - 2\eta\omega^3c_3 + \eta m_0^2\, s + 4\eta m_0\omega^2\, s - \eta\omega^2\, s\right],\\
\upsilon_0 &= \frac{1}{\Delta}(m_0R_0 - \omega S_0),\\
\nu_0 &= \frac{1}{\Delta}(\omega R_0 + m_0S_0),\\
s &= c_4 + k,\\
R_0 &= -3c_3^3 + \upsilon_1 + 2\omega\nu_1 - 2\upsilon_2,\\
S_0 &= -3sc_3^2 - 2\omega\upsilon_1 + \nu_1 - 2\nu_2,\\
m_0 &= \tfrac{1}{4} - \omega^2,\\
\Delta &= m_0^2 + \omega^2,\\
d_0 &= -c_3\mathcal{H} + c_4\omega\hat{\beta},\\
d_1 &= (c_3r - c_4\omega)\left(\mathcal{H} + \tfrac{\hat{\beta}}{2}\right),\\
\hat{\upsilon}_1 &= -\frac{3\eta(-c_3^2 + s^2)}{8\omega^2},\\
\hat{\nu}_1 &= -\frac{-3c_3\eta s}{4\omega^2},
\end{aligned}
$$

$$\hat{v}_0 = -\frac{1}{4\omega^2}\left(\tfrac{3}{2}c_3(-c_3^2+s^2) - \frac{-3c_3\eta s}{\omega}\right),$$
$$\hat{v}_0 = -\frac{1}{4\omega^2}\left(-3c_3^2\ s + \frac{3\eta(-c_3^2+s^2)}{2\omega}\right).$$

B.6. $\beta = \mathcal{O}(\varepsilon)$, *case 3*

All secular terms in $\psi_t(t)$, $\psi^3(t)$, $\phi_{0_{t\tau}}$, ϕ_{0_t}, ϕ_{0_τ}, ϕ_0^3, $\phi_0^2\,\psi(t)$ and $\phi_0\psi^2(t)$ are given follows:

$$\begin{aligned}
\psi_t(t) &: \text{ does not contain secular terms.}\\
\psi^3(t) &: \text{ does not contain secular terms.}\\
\phi_{0_\tau} &: \frac{\mathrm{d}\mathcal{A}_0(\tau)}{\mathrm{d}\tau}\mathrm{e}^{rt}\cos(\mu t) + \frac{\mathrm{d}\mathcal{B}_0(\tau)}{\mathrm{d}\tau}\mathrm{e}^{rt}\sin(\mu t).\\
\phi_{0_t} &: \left[r\mathcal{A}_0(\tau) + \mu\mathcal{B}_0(\tau)\right]\mathrm{e}^{rt}\cos(\mu t) + \left[-\mu\mathcal{A}_0(\tau) + r\mathcal{B}_0(\tau)\right]\mathrm{e}^{rt}\sin(\mu t).\\
\phi_{0_{t\tau}} &: \left[\frac{\mathrm{d}\mathcal{A}_0(\tau)}{\mathrm{d}\tau}r + \frac{\mathrm{d}\mathcal{B}_0(\tau)}{\mathrm{d}\tau}\mu\right]\mathrm{e}^{rt}\cos(\mu t) + \left[\frac{\mathrm{d}\mathcal{B}_0(\tau)}{\mathrm{d}\tau}r - \frac{\mathrm{d}\mathcal{A}_0(\tau)}{\mathrm{d}\tau}\mu\right]\mathrm{e}^{rt}\sin(\mu t).\\
\phi_0^3 &: \frac{3}{2}\left(c_3^2+c_4^2\right)\left(\mathcal{A}_0(\tau)\mathrm{e}^{rt}\cos(\mu t) + \mathcal{B}_0(\tau)\mathrm{e}^{rt}\sin(\mu t)\right).\\
\phi_0^2\psi(t) &: kc_4\left(\mathcal{A}_0(\tau)\mathrm{e}^{rt}\cos(\mu t) + \mathcal{B}_0(\tau)\mathrm{e}^{rt}\sin(\mu t)\right).\\
\phi_0\psi^2(t) &: \frac{1}{2}k^2\left(\mathcal{A}_0(\tau)\mathrm{e}^{rt}\cos(\mu t) + \mathcal{B}_0(\tau)\mathrm{e}^{rt}\sin(\mu t)\right).
\end{aligned}$$

References

[1] T. Akkaya, W.T. van Horssen, On the transverse vibrations of strings and beams on semi-infinite domains, Procedia IUTAM 19 (2016) 266–273. IUTAM Symposium Analytical Methods in Nonlinear Dynamics. https://doi.org/10.1016/j.piutam.2016.03.033

[2] T. Akkaya, W.T. van Horssen, On boundary damping to reduce the rain–wind oscillations of an inclined cable with small bending stiffness, Nonlinear Dyn. 95 (2019) 783–808. https://doi.org/10.1007/s11071-018-4596-0

[3] H. Zhou, L. Sun, F. Xing, Damping of full-scale stay cable with viscous damper: experiment and analysis, Adv. Struct. Eng. 17 (2) (2014) 265-274. https://doi.org/10.1260/1369-4332.17.2.265

[4] N.V. Gaiko, W.T. van Horssen, Resonances and vibrations in an elevator cable system due to boundary sway, J. Sound Vib. 424 (2018) 272–292. https://doi.org/10.1016/j.jsv.2017.11.054

[5] A.F. Ihsan, W.T. van Horssen, J.M. Tuwankotta, On string vibrations influenced by a smooth obstacle at one of the endpoints, J. Sound Vib. 576 (2024) 118311. https://doi.org/10.1016/j.jsv.2024.118311

[6] L. Demeio, S. Lenci, Second-order solutions for the dynamics of a semi-infinite cable on a unilateral substrate, J. Sound Vib. 315 (3) (2008) 414–432. EUROMECH colloquium 483, Geometrically non-linear vibrations of structures. https://doi.org/10.1016/j.jsv.2008.03.010

[7] M.A. Vaz, X. Li, J. Liu, X. Ma, Analytical model for axial vibration of marine cables considering equivalent distributed viscous damping, Appl. Ocean Res. 113 (2021) 102733. https://doi.org/10.1016/j.apor.2021.102733

[8] X. Liu, Y. Hu, M. Cai, Free vibration analysis of transmission lines based on the dynamic stiffness method, R. Soc. Open Sci. 6 (3) (2019) 181354. https://doi.org/10.1098/rsos.181354

[9] W.T. Van Horssen, Asymptotics for a system of nonlinearly coupled wave equations with an application to the galloping oscillations of overhead transmission lines, Q. Appl. Math. 47 (2) (1989) 197–219. https://doi.org/10.1090/qam/998096

[10] P.-T. Pham, K.-S. Hong, Dynamic models of axially moving systems: a review, Nonlinear Dyn. 100 (1) (2020) 315–349. https://doi.org/10.1007/s11071-020-05491-z

[11] K.-S. Hong, P.-T. Pham, Control of axially moving systems: a review, Int. J. Contr. Autom. Syst. 17 (12) (2019) 2983–3008. https://doi.org/10.1007/s12555-019-0592-5

[12] Darmawijoyo, On the vibrations of a linear and a weakly 1-D wave equations with non-classical boundary damping, J. Appl. Sci. 11 (7) (2011) 1206–1212. https://doi.org/10.3923/jas.2011.1206.1212

[13] E.W. Chen, N.S. Ferguson, Analysis of energy dissipation in an elastic moving string with a viscous damper at one end, J. Sound Vib. 333 (9) (2014) 2556–2570. https://doi.org/10.1016/j.jsv.2013.12.024

[14] A. Moslemi, S.E. Khadem, M. Khazaee, A. Davarpanah, Nonlinear vibration and dynamic stability analysis of an axially moving beam with a nonlinear energy sink, Nonlinear Dyn. 104 (2021) 1955–1972. https://doi.org/10.1007/s11071-021-06389-0

[15] X.-D. Yang, H. Wu, Y.-J. Qian, W. Zhang, C.W. Lim, Nonlinear vibration analysis of axially moving strings based on gyroscopic modes decoupling, J. Sound Vib. 393 (2017) 308–320. https://doi.org/10.1016/j.jsv.2017.01.035

[16] L.-Q. Chen, Analysis and control of transverse vibrations of axially moving strings, Appl. Mech. Rev. 58 (2) (2005) 91–116. https://doi.org/10.1115/1.1849169

[17] W.T. Van Horssen, On the influence of lateral vibrations of supports for an axially moving string, J. Sound Vib. 268 (2) (2003) 323–330. https://doi.org/10.1016/S0022-460X(03)00362-6

[18] N.V. Gaiko, W.T. van Horssen, On the lateral vibrations of a vertically moving string with a harmonically varying length, in: ASME International Mechanical Engineering Congress and Exposition, 57403, American Society of Mechanical Engineers, 2015, p. V04BT04A060. https://doi.org/10.1115/IMECE2015-50449

[19] N.V. Gaiko, W.T. van Horssen, On the transverse, low frequency vibrations of a traveling string with boundary damping, J. Vib. Acoust. 137 (4) (2015) 041004. https://doi.org/10.1115/1.4029690

[20] W.T. Van Horssen, On the weakly damped vibrations of a string attached to a spring mass dashpot system, J. Vib. Contr. 9 (11) (2003) 1231–1248. https://doi.org/10.1177/1077546304030699

[21] Y. Wu, E. Chen, W. Zhu, Y. He, Y. Lu, P. Chen, Vibration of an axially moving string with nonclassical boundary conditions subjected to harmonic excitation based on the method of multiple scales, Nonlinear Dyn. (2024) 1–14. https://doi.org/10.1007/s11071-023-09115-0

[22] T. Akkaya, W.T. van Horssen, On boundary damping for semi-infinite strings and beams, in: ASME International Mechanical Engineering Congress and Exposition, 57403, American Society of Mechanical Engineers, 2015, p. V04BT04A062. https://doi.org/10.1115/IMECE2015-50457

[23] B.B. Özhan, M. Pakdemirli, Principal parametric resonances of a general continuous system with cubic nonlinearities, Appl. Math. Comput. 219 (5) (2012) 2412–2423. https://doi.org/10.1016/j.amc.2012.08.048

[24] C. Kuehn, Multiple Time Scale Dynamics, 191 of *Applied Mathematical Sciences*, Springer, 2015. https://doi.org/10.1007/978-3-319-12316-5

[25] S.H. Strogatz, Nonlinear Dynamics and Chaos: With Applications to Physics, Biology, Chemistry, and Engineering, CRC Press, 2nd edition, 2015. https://doi.org/10.1201/9780429492563
[26] M. Abdi, V. Sorokin, B. Mace, On the effect of multiple incident waves on the reflected waves in a semi-infinite rod with a nonlinear boundary stiffness, in: International Conference on Wave Mechanics and Vibrations, Springer, 2022, pp. 695–702. https://doi.org/10.1007/978-3-031-15758-5_71
[27] M. Abdi, V. Sorokin, B. Mace, Reflection of waves in a waveguide from a boundary with nonlinear stiffness: application to axial and flexural vibrations, Nonlinear Dyn. 109 (4) (2022) 3051–3082. https://doi.org/10.1007/s11071-022-07584-3
[28] M. Abdi, V. Sorokin, B. Mace, Effects of incident nearfield waves on the reflection coefficients for flexural vibrations with a nonlinear boundary, J. Vib. Eng. Technol. 11 (6) (2023) 2605–2615. https://doi.org/10.1007/s42417-023-01071-8
[29] A.V. Metrikine, A.M. Kudarova, J.S. Hoving, R. van Vliet, On the minimization of wave reflection at the interface of a discrete system and a dispersively similar continuum, J. Sound Vib. 346 (2015) 191–199. https://doi.org/10.1016/j.jsv.2015.02.034
[30] W.A. Strauss, Partial Differential Equations: An Introduction, John Wiley & Sons, Hoboken, NJ, 2nd edition, Hoboken, NJ, 2007. https://books.google.nl/books?id=PihAPwAACAAJ.
[31] K.F. Graff, Wave Motion in Elastic Solids, Courier Corporation, 2012.
[32] T. Akkaya, On Boundary Damping for Elastic Structures, Dissertation (tu delft), Delft University of Technology, 2018. https://doi.org/10.4233/uuid:c463eef0-2b18-40c4-acfe-cea7399b20ea
[33] N.V. Gaiko, W.T. van Horssen, On wave reflections and energetics for a semi-infinite traveling string with a nonclassical boundary support, J. Sound Vib. 370 (2016) 336–350. https://doi.org/10.1016/j.jsv.2016.01.040
[34] S.G. Braun, D.J. Ewins, S.S. Rao, A.W. Leissa, Encyclopedia of vibration: volumes 1, 2, and 3, Appl. Mech. Rev. 55 (3) (2002) B45. https://doi.org/10.1115/1.1470670
[35] A.K. Abramian, S.A. Vakulenko, W.T. van Horssen, A. Jikhareva, The effect of small internal and dashpot damping on a trapped mode of a semi-infinite string, J. Sound Vib. 595 (2025) 118749. https://doi.org/10.1016/j.jsv.2024.118749
[36] B. Waasdorp, W.T. van Horssen, Reflections of Waves Induced by a Nonlinear Spring at the Boundary, Bachelor's thesis, Delft University of Technology, 2020. https://resolver.tudelft.nl/uuid:e5d584a1-ebb6-4a0f-8f19-f4c57f0fc13a.
[37] S. Missula, W.T. van Horssen, Wave Reflections in a Semi Infinite String Due to Nonlinear Energy Sinks at the Boundary, Master's thesis, Delft University of Technology, 2020. https://resolver.tudelft.nl/uuid:13fb65e3-7952-4aa5-bf69-b8a802396a35.
[38] H.C. Huang, Efficiency of the motion amplification device with viscous dampers and its application in high-rise buildings, Earthq. Eng. Eng. Vib. 8 (4) (2009) 521–536. https://doi.org/10.1007/s11803-009-9116-2
[39] C. Qu, G. Tu, F. Gao, L. Sun, S. Pan, D. Chen, Review of bridge structure damping model and identification method, Sustainability 16 (21) (2024). https://doi.org/10.3390/su16219410
[40] K. Lelas, I. Nakić, Optimal damping of vibrating systems: dependence on initial conditions, J. Sound Vib. 576 (2024) 118303. https://doi.org/10.1016/j.jsv.2024.118303
[41] C. Vuik, F.J. Vermolen, M.B. van Gijzen, M.J. Vuik, Numerical Methods for Ordinary Differential Equations, TU Delft Open, Delft, Delft, 2023. https://doi.org/10.5074/t.2023.001
[42] S.-Y. Lee, Jr, A generalized treatment of the energetics of translating continua, part I: strings and second order tensioned pipes, J. Sound Vib. 204 (5) (1997) 717–734. https://doi.org/10.1006/jsvi.1996.0945